ANTIMICROBIAL PROPERTIES OF 3D PRINTED SILVER NANOWIRE/POLYLACTIDE NANOCOMPOSITES

A THESIS SUBMITTED TO
THE GRADUATE SCHOOL OF NATURAL AND APPLIED SCIENCES
OF
MIDDLE EAST TECHNICAL UNIVERSITY

BY

İPEK BAYRAKTAR

IN PARTIAL FULFILLMENT OF THE REQUIREMENTS
FOR
THE DEGREE OF MASTER OF SCIENCE
IN
METALLURGICAL AND MATERIALS ENGINEERING

SEPTEMBER 2018

Approval of the thesis:

ANTIMICROBIAL PROPERTIES OF 3D PRINTED SILVER NANOWIRE/POLYLACTIDE NANOCOMPOSITES

submitted by **İPEK BAYRAKTAR** in partial fulfillment of the requirements for the degree of **Master of Science in of Metallurgical and Materials Engineering Department, Middle East Technical University** by,

Prof. Dr. Halil Kalıpçılar _____
Dean, Graduate School of **Natural and Applied Sciences**

Prof. Dr. Cemil Hakan Gür _____
Head of Department, **Metallurgical and Materials Eng.**

Prof. Dr. Hüsnü Emrah Ünalan _____
Supervisor, **Metallurgical and Materials Eng. Dept., METU**

Prof. Dr. Cevdet Kaynak _____
Co-supervisor, **Metallurgical and Materials Eng. Dept., METU**

Examining Committee Members:

Assoc. Prof. Dr. Gülçin Akca _____
Medical Microbiology Dept., Gazi University

Prof. Dr. Hüsnü Emrah Ünalan _____
Metallurgical and Materials Engineering Dept., METU

Prof. Dr. Cevdet Kaynak _____
Metallurgical and Materials Engineering Dept., METU

Assoc. Prof. Dr. Eda Ayşe Aksoy _____
Basic Pharmaceutical Science Dept., Hacettepe University

Assoc. Prof. Dr. Görkem Günbaş _____
Chemistry Dept., METU

DATE: 03.09.2018

I hereby declare that all information in this document has been obtained and presented in accordance with academic rules and ethical conduct. I also declare that, as required by these rules and conduct, I have fully cited and referenced all material and results that are not original to this work.

Name, Last Name : İpek Bayraktar

Signature :

ABSTRACT

ANTIMICROBIAL PROPERTIES OF 3D PRINTED SILVER NANOWIRE/POLYLACTIDE NANOCOMPOSITES

Bayraktar, İpek
MSc., Department of Metallurgical and Materials Engineering
Supervisor: Prof. Dr. Hüsnü Emrah Ünalan
Co-supervisor: Prof. Dr. Cevdet Kaynak

September 2018, 83 pages

Silver nanowire (Ag NW) loaded polylactide (PLA) nanocomposites were fabricated by simple solution mixing method and then 3D printed to obtain desired shapes. Morphological analysis, thermal analysis and antimicrobial performances of the fabricated nanocomposites with the addition of NWs were investigated. NWs showed good dispersion within the PLA matrix. Antibacterial properties of Ag NW/PLA nanocomposites were investigated against different standard bacterial strains of American Type Culture Collection (ATCC) using conventional microbiological methods. Ag NW based PLA nanocomposites were found to have high antibacterial effect against both *Staphylococcus aureus* ATCC#25923 (Gram positive bacteria) and *Escherichia coli* (ATCC#25922) (Gram negative bacteria). 4 wt. % Ag NW loaded nanocomposites were found to kill 100 % of *Escherichia coli* and *Staphylococcus aureus* bacteria in 2 hours and to continue its bactericidal effect for 24 hours against *Escherichia coli* and 8 hours against *Staphylococcus aureus*. Nanocomposites with higher Ag NW loadings showed better results yet small amount of Ag NW addition to PLA was found sufficient for nanocomposites to show reasonable antibacterial performance at low cost.

Keywords: 3D printing, PLA based nanocomposites, biomaterials, antibacterial materials, polylactide, nanowires

ÖZ

ÜÇ BOYUTLU YAZICILARLA BASILMIŞ POLİLAKTİT/GÜMÜŞ NANOTEL NANOKOMPOZİTLERİN ANTİMİKROBİK ÖZELLİKLERİ

Bayraktar, İpek

Yüksek Lisans, Metalurji ve Malzeme Mühendisliği Bölümü

Tez Yöneticisi: Prof. Dr. Hüsnü Emrah Ünalan

Ortak Tez Yöneticisi: Prof. Dr. Cevdet Kaynak

Eylül 2018, 83 sayfa

Bu çalışmada gümüş nanotel katkılı polilaktik asit (PLA) bazlı nanokompozitler çözelti karıştırma yöntemiyle üretilmiş ve üç boyutlu yazıcılarla istenilen şekillerde basılmıştır. Üç boyutlu yazıcılarla basılmış numunelerin morfolojik, termal ve antimikrobik özelliklerinin eklenen gümüş nanotel miktarıyla değişimi incelenmiştir. Nanotellerin polimer matris içerisinde homojen dağılımı gözlenmiştir. Nanokompozitlerin antimikrobik özellikleri konvensiyonel mikrobiyolojik yöntemler kullanılarak farklı bakteri suşlarına karşı araştırılmıştır. Gümüş nanotel bazlı PLA nanokompozitlerin hem *Staphylococcus aureus* (Gram-pozitif bakteri) hem de *Escherichia coli* (Gram-negatif bakteri) karşısında yüksek antibakteriyel etkiye sahip olduğu gözlenmiştir. Kütlece %4 gümüş nanotel katkılı nanokompozitlerinin *Escherichia coli* ve *Staphylococcus aureus* bakterilerini iki saatte %100 öldürdüğü ve bu bakteri öldürücü etkinin *Escherichia coli* için 24 saat *Staphylococcus aureus* için 8 saat sürdüğü görülmüştür. Daha yüksek gümüş nanotel katkılarının daha iyi sonuçlar ortaya koyduğu bulunmuş ancak düşük katkılarla da makul antibakteriyel özelliklerin sağlandığı saptanmıştır.

Anahtar Kelimeler: Üç boyutlu yazıcılar, PLA bazlı nanokompozitler, biomalzemeler, antibakteriyel malzemeler, polilaktit, nanoteller

In memory of my uncle Olcay Atalay

ACKNOWLEDGEMENTS

Firstly, I would like to express my sincere gratitude to my supervisor Prof. Dr. Hüsnü Emrah Ünalan for his continuous support, guidance, motivation and patience throughout this study. Also, I thank my co- advisor Prof. Dr. Cevdet Kaynak for his valuable support, and immense knowledge. Besides my advisors, I am deeply grateful to Assoc. Prof. Dr. Gülçin Akca and her group members, our collaborators in Gazi University, for their unlimited assistance, technical contribution, insightful comments and positive approach.

Moreover, I would like to thank TÜBİTAK, the Scientific and Technological Research Council of Turkey, for their financial support via "Priority Fields Support Program (2210-C)", and Middle East Technical University, Scientific Research Projects programme for their financial support during this work (BAP-07-02-2015-008 and BAP-07-02-2017-004-263).

Also, I would like to thank Şahin Coşkun and Doğa Doğanay, my mentors in this thesis, for their guidance and support, and my lab mates, Alptekin Aydınlı, Elif Güner, Doğancan Tigan, Selin Özkul, Serkan Koylan, Mete Batuhan Durukan, Sevim Polat, Yusuf Tutel, Şeyma Koç, Şensu Tunca, Efe Boyacıgiller, Ece Alpugan. I also would like to thank Ulaş Can, Eren Erol, Yelda Meyva, Deniz Varsavaş and Burcu Sarı for their support and friendship during this project.

I owe my profound gratitude to my dearest friends; Elif Agah, Gizem Aslan, Elif Bilgiç for their unlimited support, and motivation through this project. Most importantly, I would like to express my special appreciation to Erdi Kandemir for his guidance, patience and moral support.

Lastly, I am deeply grateful to my dearest family for their encouragement, understanding, unconditional support. This thesis would have never been completed without them.

TABLE OF CONTENTS

LIST OF TABLES

LIST OF FIGURES

ABBREVATION LIST

AM: Additive Manufacturing

$AgNO_3$: Silver Nitrate

Ag NP: Silver Nanoparticle

Ag NW: Silver Nanowire:

B. cereus: Bacillus cereus

CAD: Computer Aided Design

C. albicans: Candida albicans

DSC: Differential Scanning Calorimetry

E. coli: Escherichia coli

EG: Ethylene glycol

FDM: Fused Deposition Modelling

HNT: Halloysite Nanotube

LA: Lactide

LOM: Laminated Object Manufacturing

NaCl: Sodium Chloride

PLA: Poly(lactic acid) or polylactide

ROP: Ring-opening Polymerization

S. aureus: Staphylococcus aureus

SEM: Scanning Electron Microscopy

SLA: Stereolithography

SLM: Selective Laser Melting

SLS: Selective Laser Sintering

$Sn(Oct)_2$: Tin octoate

TGA: Thermogravimetric Analysis

TEM: Transmission electron microscopy

CHAPTER 1

INTRODUCTION

3D printing as a subset of additive manufacturing has received a great deal of attention in the last few decades with potential uses in various industries. Reduction of mass and manufacturing costs, ability to produce complex products with high precision [1], significant reduction in the lead time, elimination of additional processes and highly flexible design of structures are just some of the advantages of additive manufacturing that make it superior over conventional manufacturing [2]. Due to its advantages, application field of additive manufacturing expanded rapidly especially in aerospace and defence, automotive, healthcare and consumer product industries [3]. There are different types of additive manufacturing techniques. Fused deposition modelling (FDM) is one of the most widely used additive manufacturing method, which is suitable for the fabrication of thermoplastic polymers such as polylactide (PLA) [4]–[6] and acrylonitrile butadiene styrene (ABS) [4], [5], [7].

It can be stated that PLA can be one of the most appropriate ink candidates in 3D printing because of its physical properties. Moreover, PLA has significant advantages such as environmentally friendly character, promising thermomechanical properties, perfect biocompatibility and degradability [8]. These advantages allow PLA to be utilized in a wide range of applications especially in biomedical, food and beverage packaging as well as in tissue engineering [9].

Despite its advantages, 3D printed bare polymer products, especially bare PLA generally suffer from strength and functionality that restrict its industrial applications. Therefore, these products can only be used as conceptual prototypes in the fields of architecture [14], education, medicine [16] and art fields [15].

However, it can gain functionality by improving its properties with some additives in nanocomposite form. For this purpose, polymer based nanocomposites takes considerable attention due to their promising mechanical, electrical, physicochemical and structural properties. Fabricating polymer nanocomposites by additive manufacturing, both facilitates building structures in a fast, easy way with higher precision compared to conventional composite fabrication techniques and produces functional products with excellent properties rather than simply 3D printed bare polymers. Therefore, 3D printing of nanocomposites combines of process flexibility and functionality of products [1].

3D printing of polymer nanocomposites has been extensively studied in the recent years. Until now, metal nanoparticles, metal nanowires, carbon nanotubes (CNTs) and ceramic nanoparticle filled polymer matrix nanocomposites were examined [1], [10]. Metal nanoparticles such as Ag NPs were found to improve the electrical properties of the polymer matrix whereas CNTs provided high tensile strength with good dispersion in polymer matrix that results in mechanically improved nanocomposites. Moreover, ceramic nanoparticles have also been investigated as nanofillers in 3D printing. With the addition of titanium oxide (TiO_2) nanoparticles, tensile strength, flexural strength and hardness values of the nanocomposites were improved [11]. In addition to these, thermal stability was also improved with the addition of TiO_2 nanoparticles due to their high thermal stability.

For centuries, Ag and Ag compounds have been known as high performance antimicrobial materials [12]. They have been used both in the treatment of human diseases and the disinfection of medical devices [13], [14]. It is also well known that metal particles including Ag show advanced physical properties in nanoscale mainly caused by the increase in the surface to volume ratio [15], [16]. Therefore, Ag nanomaterials especially Ag nanoparticles have received great attention with time and have taken the place of Ag in bulk form for the healthcare industry. Their antimicrobial properties particularly in polymer matrices have been studied the most in literature [17], [18].

In this study, Ag NWs are used for the first time as nanofillers in 3D printing. It has been aimed to fabricate functional Ag NW/PLA nanocomposites with antimicrobial properties using a commercially available 3D printer. For this purpose, Ag NW/PLA nanocomposites were fabricated by solution mixing method and 3D printed using Ultimaker 2+, a FDM type 3D printer. Then, antibacterial properties of 1, 2, 4 wt. % Ag NW loaded nanocomposites were investigated and the effects of Ag NW loadings were examined against both *Staphylococcus aureus* and *Escherichia coli*.

CHAPTER 2

LITERATURE REVIEW

2.1. 3D Printing Technology

2.1.1. Introduction to 3D Printing

Additive manufacturing (AM) as the superset of 3D printing is a manufacturing technique where materials are joined layer by layer to fabricate complex geometries based on CAD models. It was first described by Charles Hull in 1986 as a process called stereolithography (SLA) [19] and different methods were developed over the years. Rapid prototyping, reducing printing defects, ability to print structures with high precision and resolution are the key parameters in the development of additive manufacturing technologies. Fused deposition modelling (FDM), selective laser melting (SLM), selective laser sintering (SLS), inkjet printing, liquid binding in three dimensional printing (3DP), stereolithography (SLA) and laminated object manufacturing (LOM) can be listed as principal additive manufacturing methods [20].

The main conceptual difference of AM from subtractive and formative manufacturing is that material is added layer by layer to form 3D structures in AM instead of machining or casting a bulk material, as can be seen in Figure 2.1 [21].

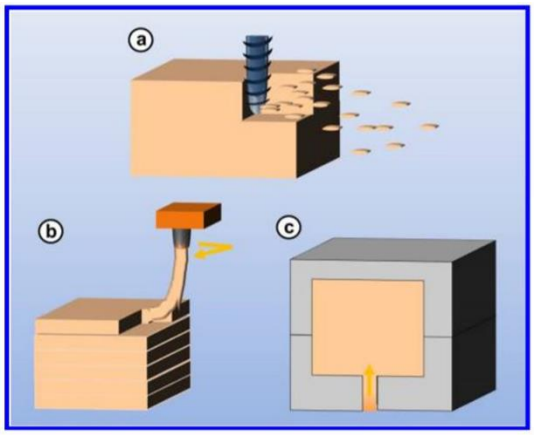

Figure 2.1. Schematic illustrations of (a) subtractive, (b) additive and (c) formative manufacturing techniques [21].

Additive manufacturing process flow starts with a CAD based 3D model as demonstrated in Figure 2.2. Firstly, 3D model is converted into (.stl) file and uploaded to the printer software. Then, data file is sliced into layers by this software. Material is extruded layer by layer on top of the previous layer by the 3D printer. After final product is completely built, post process treatments are performed where necessary [3].

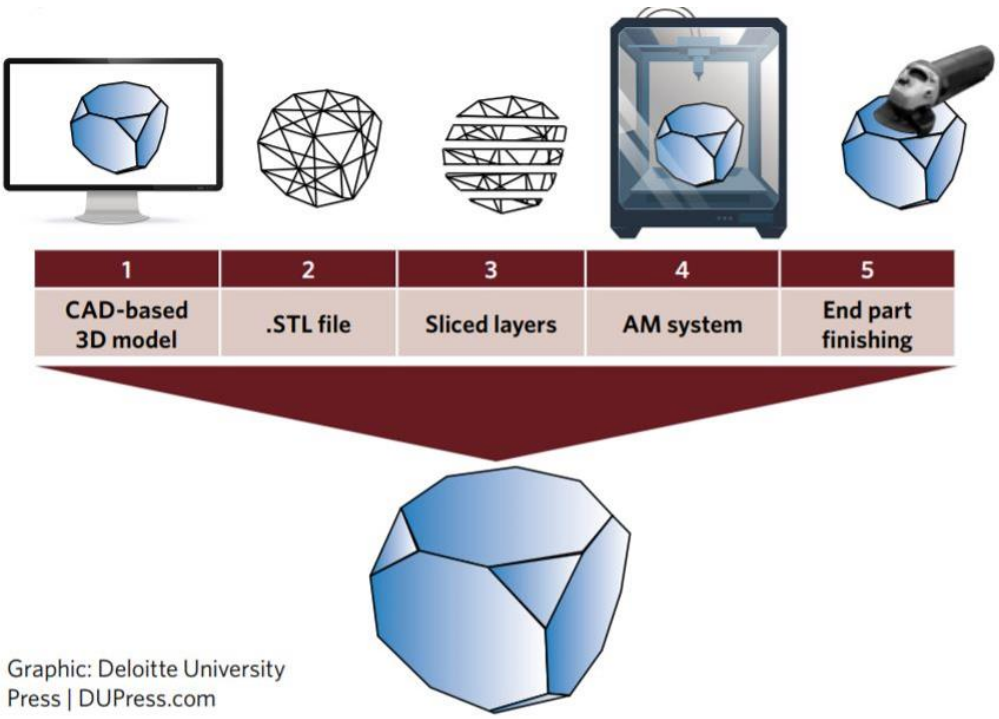

Figure 2.2. AM process flow [3].

AM offers lots of advantages that makes it outstanding over traditional manufacturing processes. Firstly, AM enables producing complex shaped materials with high precision, which is difficult to achieve with subtractive manufacturing. Moreover, AM produces final prototypes without any machining or joining processes. Elimination of additional processes results in time, cost and energy savings. Also, waste and scrap are reduced in AM as it is based on adding material layer by layer as opposed to subtractive manufacturing which consists of machining and drilling processes [3].

In addition to these advantages, there are some specific benefits of traditional manufacturing that AM cannot provide yet. At first, AM is not suitable for high volume production as opposed to traditional manufacturing. In addition, AM limits the types of materials to be used while a wide range of material types can be used in traditional manufacturing. Furthermore, manufacturing of large components is not possible with AM, since the dimensions of the products are restricted by the printer bed size. Therefore, traditional manufacturing is much more advantageous in the fabrication of large components. Each AM method has its own characteristics, advantages, disadvantages and application areas [3]. They are explained in detail in the following part.

2.1.2. Main 3D Printing Methods

2.1.2.1. Fused Deposition Modelling (FDM)

FDM is the most commonly used method developed in late 1980's for polymer and polymer based composite materials [22]. Especially thermoplastic polymers such as polylactide (PLA), acrylonitrile butadiene styrene (ABS), polycarbonate (PC) are preferred as inks for their low melting temperatures. In FDM, material is heated up to a temperature just above the melting temperature of the material and melted to a semi-liquid phase. Then, filaments are extruded layer by layer on printer plate on top of each other. Layers are fused together and solidify into the final product at room temperature [1], [20]. Figure 2.3 shows the FDM process and ongoing physical phenomena in depth including material flow, flow and fiber orientation, bond formation on deposited material and solidification behavior [23].

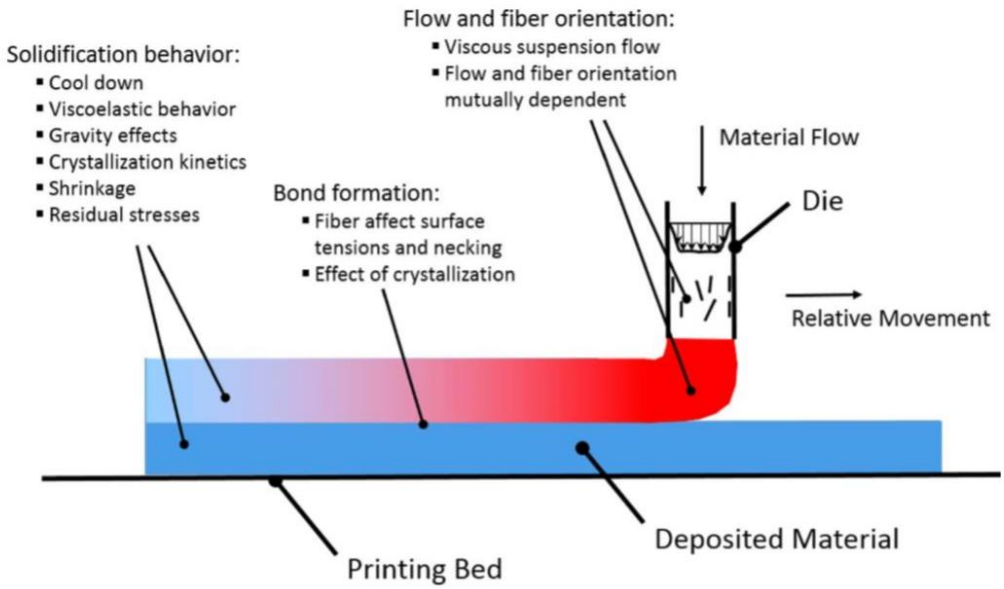

Figure 2.3. Schematic illustration of FDM process and the ongoing physical phenomena during printing [23].

Mechanical properties of the final products can be arranged by changing printing parameters like infill content, printing pattern, layer thickness and air gap [24]. Effects of these parameters were discussed in detail by Sood et al. [25].

Ease of process, high speed, low cost and accessibility of FDM printers are the advantages of this process that makes it the most preferred technology in 3D printing. However, some drawbacks such as poor surface quality [26], low resolution, limited number of suitable materials weakens mechanical properties of the final product and restricts application area of FDM method [24]. Moreover, material should be in filament form to be extruded in FDM. Homogenous dispersion of reinforcements in polymer matrix and preparation of composite filaments can sometimes be difficult.

2.1.2.2. Powder Bed Fusion

Powder bed fusion technology was first found in 1993 at Massachusetts Institute of Technology (MIT). This technology is based on spreading fine powders on build platform through layer by layer and fusing them on top of each other with the help of a laser beam or a liquid binder as illustrated in Figure 2.4 [27]. Laser beam is used for materials with low melting or sintering temperatures, while binder is used only for materials with high melting temperatures. Once the final product is completely built, remaining excess powder is removed from body. Finally, if necessary surface plating, coating, sintering can be performed according to the material used [20].

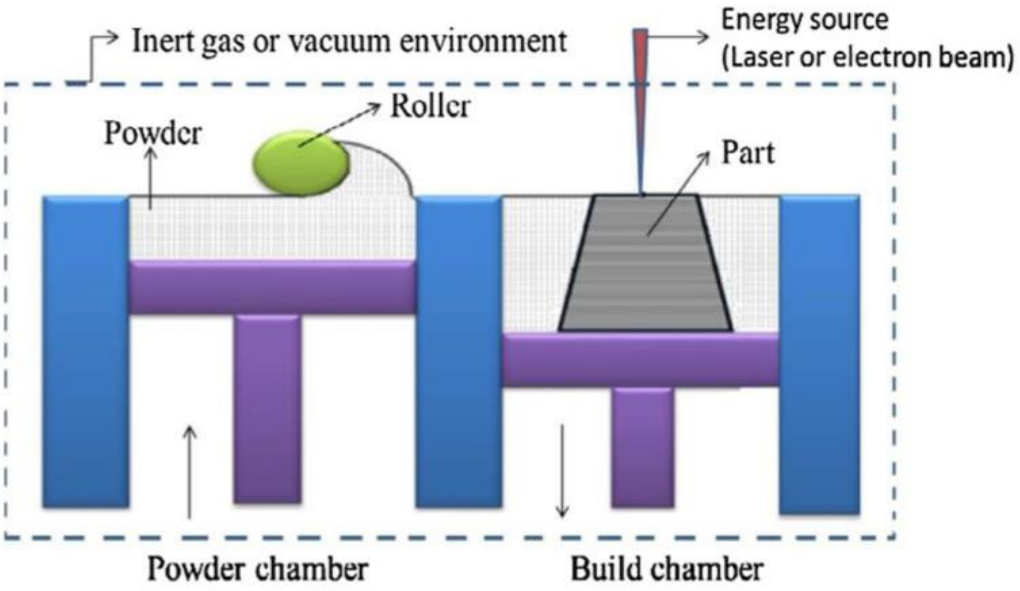

Figure 2.4. Schematic illustration of powder bed fusion [27].

Selective Laser Melting (SLS) is generally preferred for thermoplastic polymers, ceramic and metal powders. In this method, a laser helps to fuse the powders by providing thermal energy for powder sintering by partial melting [2]. On the other hand, selective laser melting (SLM) is used for metals such as stainless steels, aluminum and tool steels. Metal powders are fully melted by the laser beam different from SLS. This provides a final product with excellent mechanical properties [28].

Process parameters like powder size distribution, chemistry of the binder, binder viscosity, interaction between binder and powder, binder deposition speed determine the efficiency of power bed fusion processes and properties of the final product [1], [29].

Effects of process parameters on the final product were studied by Ben et al. [29]. This method is used in tissue engineering, aerospace and electronics due to its numerous number of advantages. Fine resolution of the printed product, flexibility of the material used, room temperature processability, high surface quality are the main advantages of this method, all of which make it very suitable for advanced applications. However, use of a binder sometimes causes porous final product and also can lead to contaminations. Moreover, it is a slow process with high cost. Thus, this method is only preferred in advanced industries [1], [20].

2.1.2.3. Stereolithography (SLA)

Stereolithography is the oldest 3D printing method developed in 1986 and still one of the most preferred technique among all solid freeform techniques [30]. This method is based on polymerization of UV-active monomers by UV laser or electron beam into a 2D patterned layer. After one layer is cured, platform is moved downward and next layer is patterned on top of the previous one. This process is repeated until a 3D model is formed. At the end of printing, post process treatments such as polishing, finishing, painting may be required in order to improve the surface quality. In addition, photocuring in a UV oven may be carried out in order to complete polymerization and enhance mechanical properties of the final product [20], [31]. Figure 2.5 schematically shows the SLA process in detail [32].

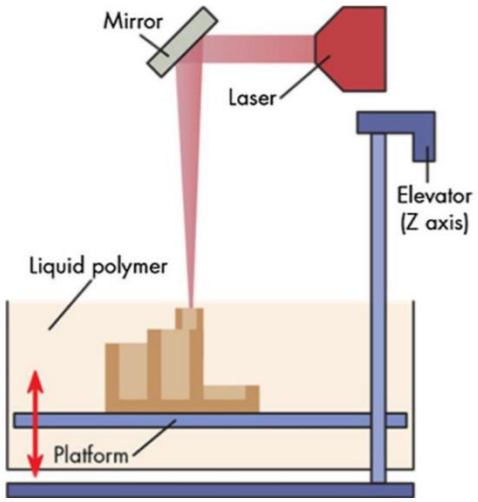

Figure 2.5. Schematic illustration of SLA process [32].

Intensity and the power of the laser, scan speed and exposure time are the main process parameters affecting printing resolution and quality of the final prototype [33]. Existence of photoinitiators and UV absorbers are also effective in SLA process as they control the depth of polymerization [34].

Main advantage of SLA is the formation of high quality products with fine resolution down to 10 μm [1]. Also, being a nozzle free technique is an important advantage of SLA that eliminates all the clogging related problems during printing [1]. However, it is a slow and expensive process. Moreover, maximum printable product size is relatively small, suitable material types for SLA are limited when compared with other 3D printing technologies. Also, curing process has lots of control parameters that makes SLA complex for basic applications [30], [35]. Based on the advantages and disadvantages listed above, SLA can be used for the fabrication of complex polymer nanocomposites [36].

2.1.2.4. Laminated Object Manufacturing (LOM)

Laminated object manufacturing technology consists of both subtractive and additive manufacturing steps differently from other AM technologies [35]. It is based on cutting initial material layer by layer and bonding printed layers as shown in Figure 2.6. Layers are firstly cut by mechanical cutters or a laser beam and bonded together by pressure and heat or vice versa according to the material type. For example, form-then-bond method is more favorable for metallic and ceramic materials since forming process may be more effortful after thermal bonding of layers. Once cutting and bonding are completed, excess material can be easily removed from the body. Post processing treatments can be performed according to the material type and desired properties [20].

Polymer composites, metals, papers, fabrics can be fabricated by LOM. Moreover, ultrasonic additive manufacturing (UAM), recently developed subgroup of LOM, enables metallic materials to be manufactured at low temperatures that is not possible with other AM technologies. LOM offers great potential in paper manufacturing, foundry, electronics including sensor applications [20], [35].

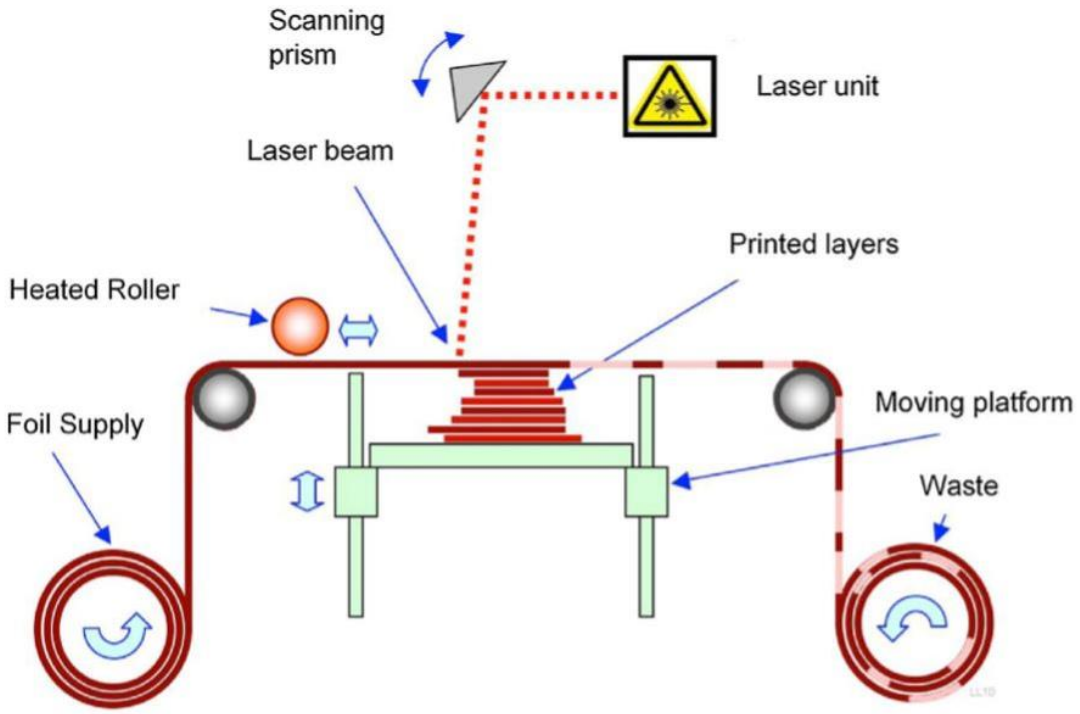

Figure 2.6. Schematic illustration of LOM process [32].

LOM provides elimination of machining steps and so results in the reduction of both manufacturing costs and lead time. Moreover, any phase change or deformation on the material is not observed during the process. These advantages enable this technology to be one of the most commonly used method in manufacturing of large components. However, it is not recommended for complex shaped components because of the drawbacks of LOM, such as poor surface finish and resolution, low dimensional accuracy especially in z-axis and time consuming excess material removal after printing [20], [35], [37].

Table 2.1 summarizes materials, applications, advantages and drawbacks of additive manufacturing.

Table 2.1. Summary of materials, applications, benefits and drawbacks of additive manufacturing methods [20].

Methods	Materials	Applications	Benefits	Drawbacks	Resolution range (μm)
Fused deposition modelling	Continues filaments of thermoplastic polymers Continuous fibre-reinforced polymers	Rapid prototyping Toys advanced composite parts	Low cost High speed Simplicity	Weak mechanical properties Limited materials (only thermoplastics) Layer-by-layer finish	50-200 μm [13]
Powder bed fusion (SLS, SLM, 3DP)	Compacted fine powders Metals, alloys and limited polymers (SLS or SLM) ceramic and polymers (3DP)	Biomedical Electronics Aerospace Lightweight structures (lattices) Heat exchangers	Fine resolution High quality	Slow printing Expensive High porosity in the binder method (3DP)	80-250 μm [13]
Stereolithography	A resin with photo-active monomers Hybrid polymer-ceramics	Biomedical Prototyping	Fine resolution High quality	Very limited materials Slow printing Expensive	10 μm [13]
Laminated object manufacturing	Polymer composites Ceramics Paper Metal-filled tapes Metal rolls	Paper manufacturing Foundry industries Electronics Smart structures	Reduced tooling and manufacturing time A vast range of materials Low cost Excellent for manufacturing of larger structures	Inferior surface quality and dimensional accuracy Limitation in manufacturing of complex shapes	Depends on the thickness of the laminates

2.2. 3D printed PLA based Nanocomposites

2.2.1. Polylactide (PLA)

PLA was firstly synthesized in 1845 by condensation of L-lactic acid and commercialized after 1990 [9],[38]. The monomer lactic acid with high purity is obtained by fermentation of corn or sugar. Purity of LA is important for high quality production of PLA. Ring opening polymerization (ROP) of LA using tin octoate ($Sn(Oct)_2$) as catalyst and chemical structures of two isomers of lactic acid, D-lactic acid and L-lactic acid [39] are given in Figure 2.7 [40].

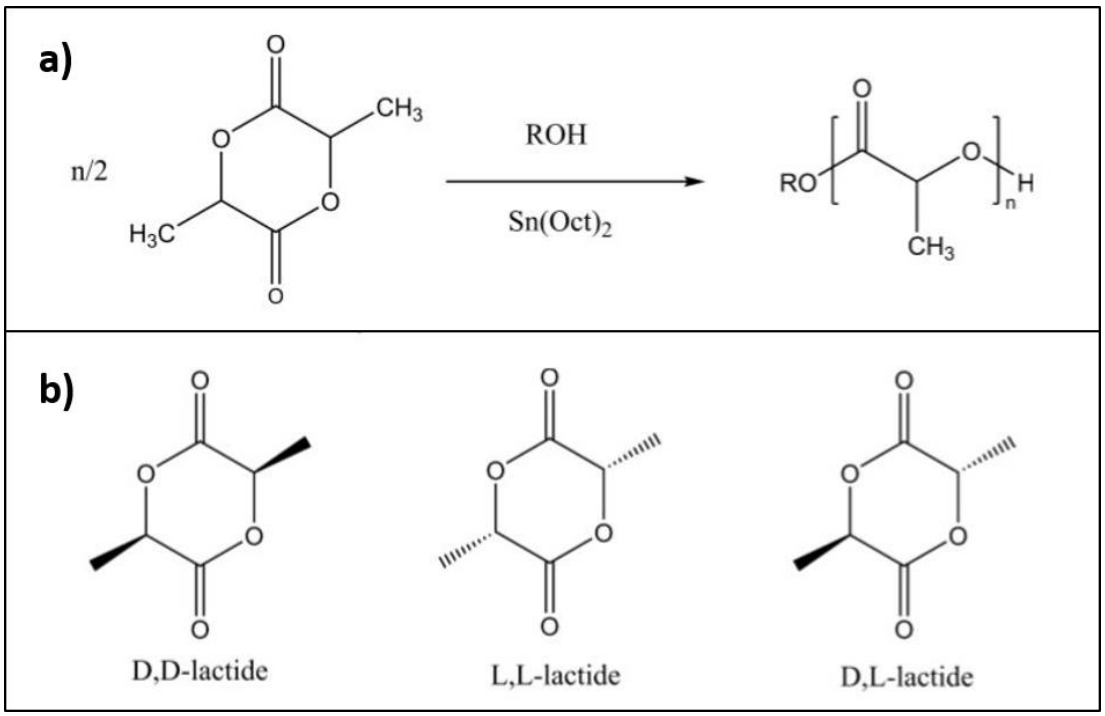

Figure 2.7. (a) Chemical structures of ROP of LA with ROH/ $Sn(Oct)_2$ and (b) chemical structures of LA isomers [40].

There are two main methods of producing PLA, which are direct polycondensation reaction and ring opening polymerization of lactide monomer. Low molecular weight PLA is produced by first method due to water formed during reaction. [41]–[45]. Therefore, polycondensation has been replaced with ring- opening polymerization (ROP) of LA developed by Nature Works LLC (Cargill Dow LLC) [9].

In this process, firstly pre polymer LAs are formed by condensation. Then, high molecular weight PLA is obtained via ROP with $Sn(Oct)_2$ as catalyst. [46]. Two methods of PLA production are summarized schematically in Figure 2.8. Ratio of LA monomer (L and D) used in production determines the final properties of PLA [9].

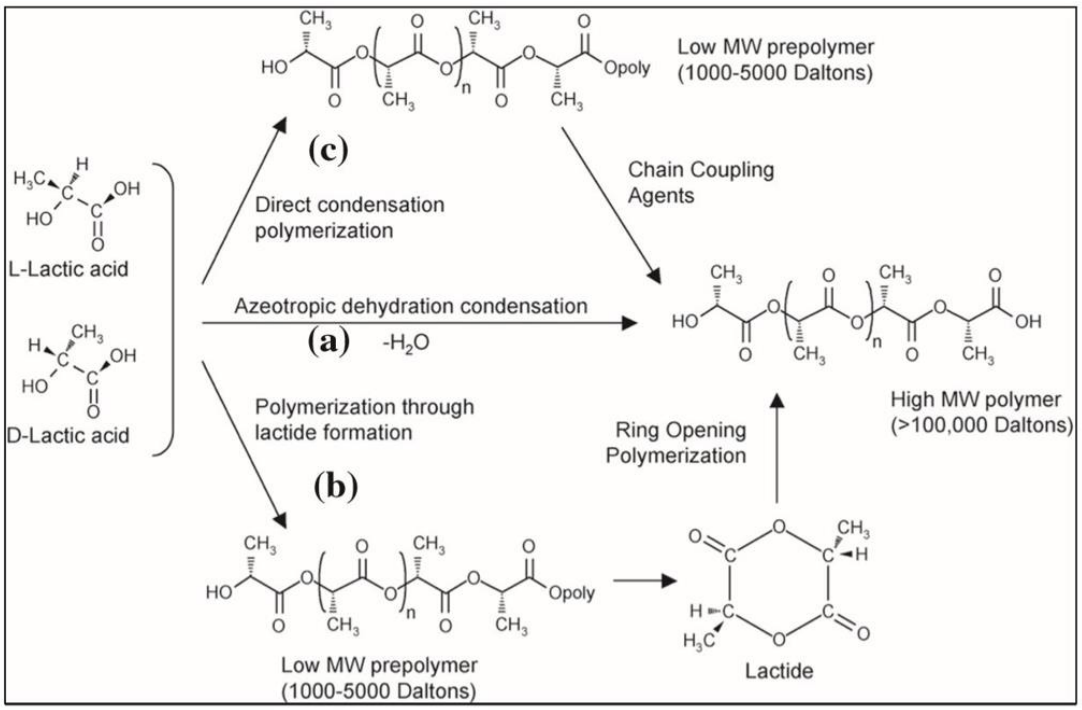

Figure 2.8. Polymerization methods of PLA production [84].

PLA has numerous characteristic properties, such as high stiffness and rigidity, suitability to several process conditions, shiny appearance. All the properties differ PLA from other polymers.

Mechanical properties of semicrystalline PLA is highly dependent on its molar mass and degree of crystallinity [47]–[50]. Its tensile modulus and flexural modulus values are approximately 3 GPa and 5GPa, respectively. Moreover, tensile strength and flexural strength of PLA is around 40-70 MPa and 100 MPa, respectively [51], [52]. The two most important thermal properties of PLA are the glass transition and melting temperatures, which are in the range of 45-60 °C and 150-162 °C, respectively [53].

2.2.2. 3D printed PLA based nanocomposites

PLA is the most commonly used polymer ink in 3D printing due to a few reasons explained before. However, properties of 3D printed bare PLA cannot meet the requirements for most applications especially when mechanical strength is desired. Therefore, the mechanical properties 3D printed PLA based structures should be enhanced by loading fillers. The use of nanofillers provide substantial enhancements to polymer matrix even at low filler fractions. For this reason, 3D printing of nanocomposites evolved as an important research field. In this section of the thesis, 3D printed PLA based nanocomposites reported to date are discussed.

2.1.2.1. Poly(lactic acid)/Graphene Nanacomposites

Graphene is one of the most attractive candidates to be used as nanofiller due to its excellent mechanical, electrical and thermal properties [54]. In Prashantha and Roger's study, commercial 10 wt.% PLA/graphene nanocomposites were 3D printed by FDM technology using Makerbot Replicator 2 printer. Mechanical, electrical and electromagnetic induction shielding properties of 3D printed samples were evaluated [55]. It was found that graphene nanoplatelets remarkably enhance the mechanical properties as shown in Figure 2.9 (a). Elastic modulus was increased by 30% and ultimate tensile strength was improved by 27% compared to bare PLA. Samples were printed horizontally in order to align graphene nanoplatelets in the direction of load resulting in maximized mechanical strength.

Moreover, dynamic mechanical analysis of PLA and 3D printed nanocomposite were examined. It was realized that graphene enhances the storage modulus of PLA matrix by about 25% and shift DMA curve upwards as shown in Figure 2.9 (b).

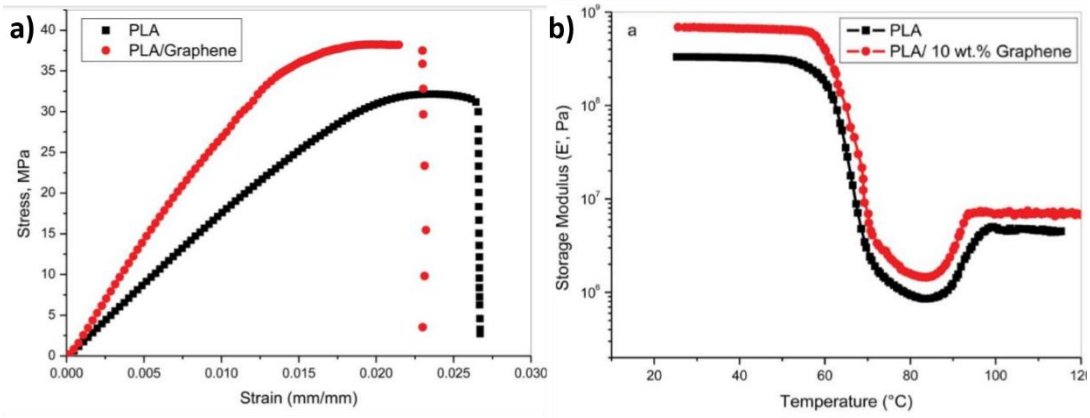

Figure 2.9. (a) Stress-strain curve of 3D printed PLA and PLA/graphene nanocomposites. (b) Storage modulus of 3D printed PLA and PLA/graphene nanocomposites as a function of temperature [55].

In another study, Bustillos et al. analyzed creep and wear resistance of 3D printed PLA/graphene nanocomposites. For this purpose, commercial bare PLA and PLA/graphene nanocomposite filaments were fabricated by FDM printer. Firstly, hardness of printed samples was evaluated. PLA/graphene nanocomposites exhibited higher resistance to surface indentation (146 MPa) compared to bare PLA (123 MPa). Moreover, the creep resistance of bare PLA was improved by 20.5% at a load of 90 mN as shown in Figure 2.10 and strain rate sensitivity index was found as 0.21 for PLA/graphene nanocomposites and 0.11 for bare PLA. These results proved that PLA/graphene nanocomposites can be used as scaffolds for orthopedic applications [56].

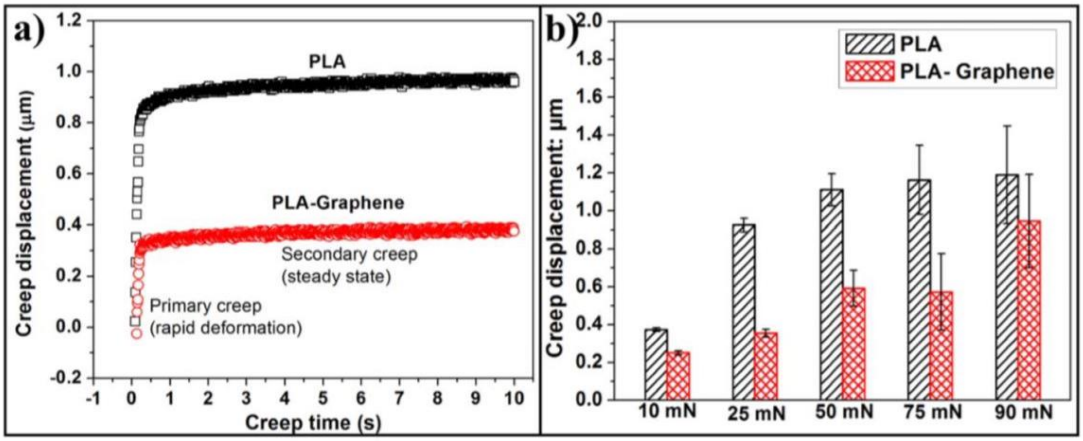

Figure 2.10. (a) Creep displacement-time curves of 3D printed PLA and PLA/graphene nanocomposites. (b) Creep displacement at different loads [56].

2.1.2.2. Poly(lactic acid)/ Carbon Nanotube(CNT)

Conductive polymer nanocomposites are highly promising for sensors, antistatic packaging and electromagnetic interference (EMI) shielding applications. Carbon nanotubes (CNTs) are the most widely used nanofillers in the fabrication of conductive nanocomposites (CNCs). Besides conventional fabrication methods of CNC's such as solvent-casting, compression molding and injection molding, 3D printing has stepped forward in literature.

In Chizari's study, PLA/CNT highly conductive nanocomposites were fabricated via ball milling method and scaffold structures used as liquid sensors with different parameters were printed by solvent cast 3D printing method [57]. The effects of structural parameters; filament diameter, inter-filament spacing (IFS), thickness of scaffolds, configuration patterns on sensitivity of liquid sensors were investigated. Results obtained regarding relative resistance change (RRC) with four structural parameters were demonstrated in Figure 2.11.

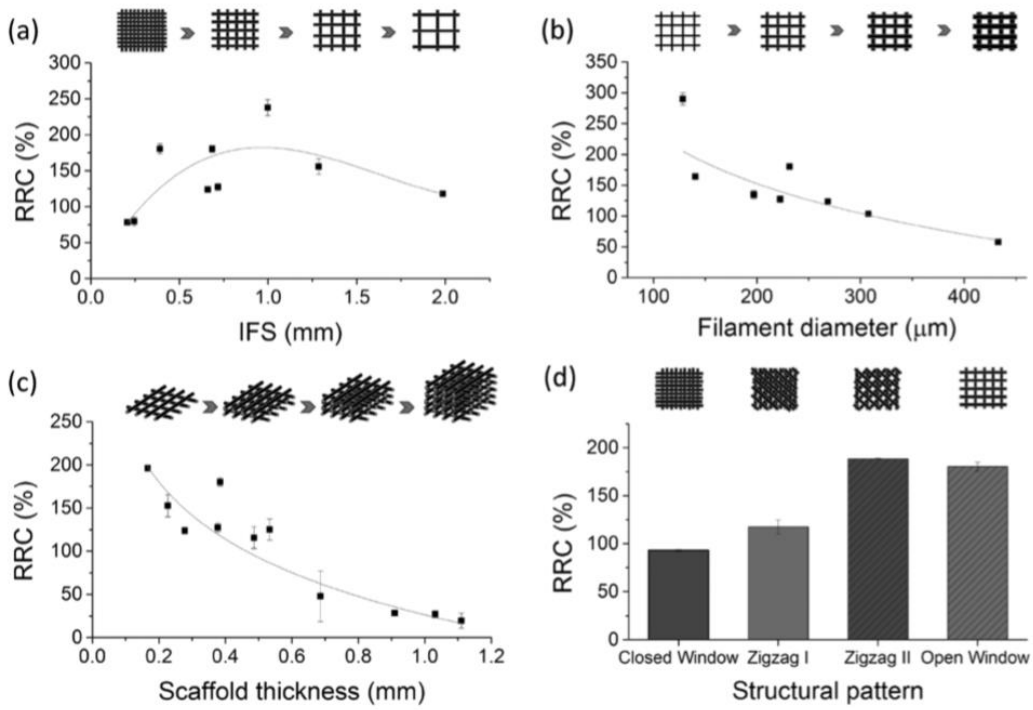

Figure 2.11. The effect of (a) inter filament spacing, (b) filament diameter, (c) scaffold thickness, and (d) structural patterns on the RRC [57].

Higher RRC values are desired for sensor applications since they increase the sensor sensitivity. Therefore, these results showed that optimum values were obtained with IFS between 0.5 and 1.5 mm, filament diameter <250 μm, thickness <0.6 mm. Based on the results, it can be summarized that this technology can be used for gas and strain sensing. In addition, It was considered to be highly suitable for EMI shielding and electronics in 3D circuits.

2.1.2.3.Poly(lactic acid)/Clay Nanacomposites

Clay, as a one of the most widely used nanofiller especially for polymer matrix composites has been also studied in 3D printing technology. In 2017, Coppola and co-workers investigated the effects of layered silicates on mechanical and thermal properties of 3D printed PLA. PLA/clay nanocomposites were fabricated and filaments were prepared by sequential extrusion processes [58].

DSC thermographs provided in Figure 2.12 shows that the glass transition of PLA remained almost constant around 60 °C. On the other hand, crystallization temperature of PLA decreased by 12% since nanoclays act as nucleating agents and promote PLA crystallization. Moreover, mechanical properties were also examined in this study. According to dynamic mechanical testing results, 15% enhancement in elastic modulus was obtained in 3D printed PLA/clay nanocomposites with 4 wt.% nanoclay addition.

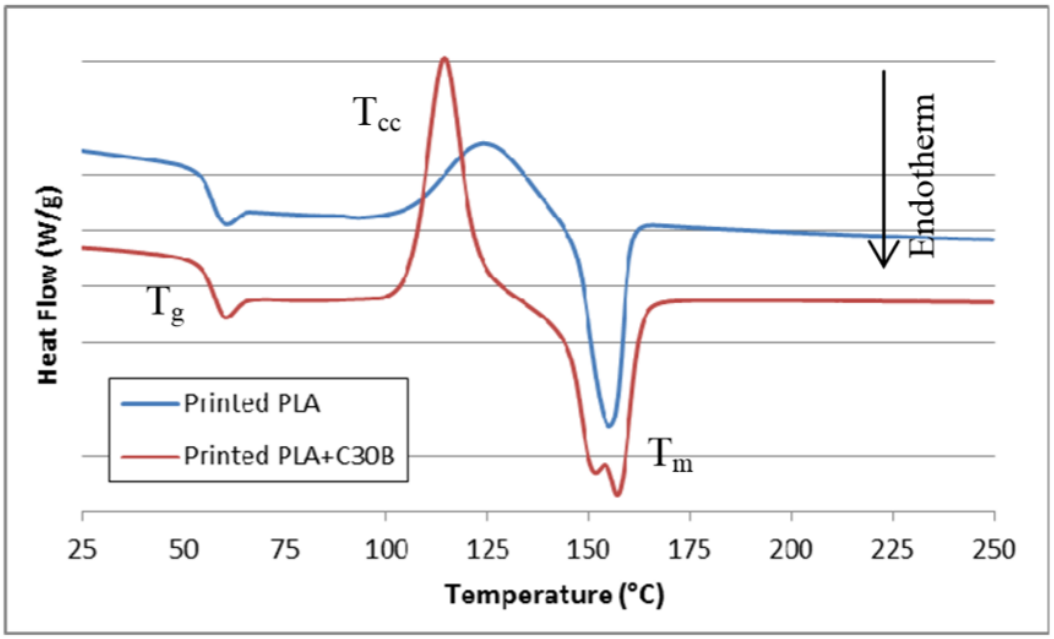

Figure 2.12. First heating thermographs of 3D printed bare PLA and PLA/clay nanocomposites [58].

2.3 Antibacterial Ag Nanoparticle (Ag NP) Loaded Nanocomposites

2.3.1. Silver as an Antibacterial Agent

Metal and metal oxide nanoparticles including silver (Ag), titanium oxide (TiO_2), zinc oxide (ZnO) and iron oxide (Fe_3O_4) are well known for their antimicrobial activities [59]. Over a wide range of nanomaterials, Ag has attracted great interest because of its strong inhibitory and bactericidal effects against bacteria, fungi and viruses [60].

2.3.2. Bacterial Membrane Damage by Silver

Ag NPs are firstly attached and start to accumulate on the surface of bacterial cell wall when interacted with the bacteria cells. Penetration of Ag in to cell results in the deterioration of the integrity of bacterial membrane and change the permeability of the cell wall. This causes leakage of bacterial contents (i.e. reducing sugars and proteins), damage the membrane and results in cellular death [12], [61]–[63].

In Li's study, influence of Ag NPs on the leakage of reducing sugars and proteins from *Escherichia coli (E.coli)* cells were investigated to reveal bacterial membrane damage [61]. It was realized that Ag NPs increase the membrane permeability and improve leakage of reducing sugars and proteins from bacteria cells as demonstrated in Figure 2.13.

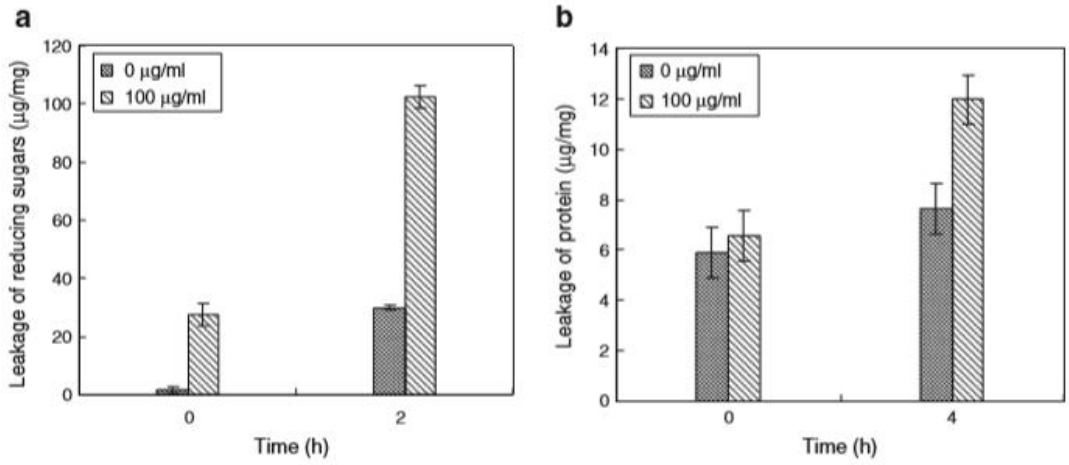

Figure 2.13. (a) Leakage of reducing sugars and (b) proteins from *Escherichia coli* cells treated with and without Ag NPs [61].

Moreover, microstructures of *E. coli* cells were examined via scanning electron microscope (SEM) and transmission electron microscope (TEM) in order to reveal morphological changes in the same study. In the SEM images provided in Figure 2.14 (a, b), cells treated with Ag NPs were found to be shapeless and fragmentary. Also, in TEM images shown in Figure 2.14 (c) and (d), many pits and gaps was observed on the cell membrane. Based on these micrographs, it was summarized that Ag NPs damaged bacteria cells severely resulting in cell death.

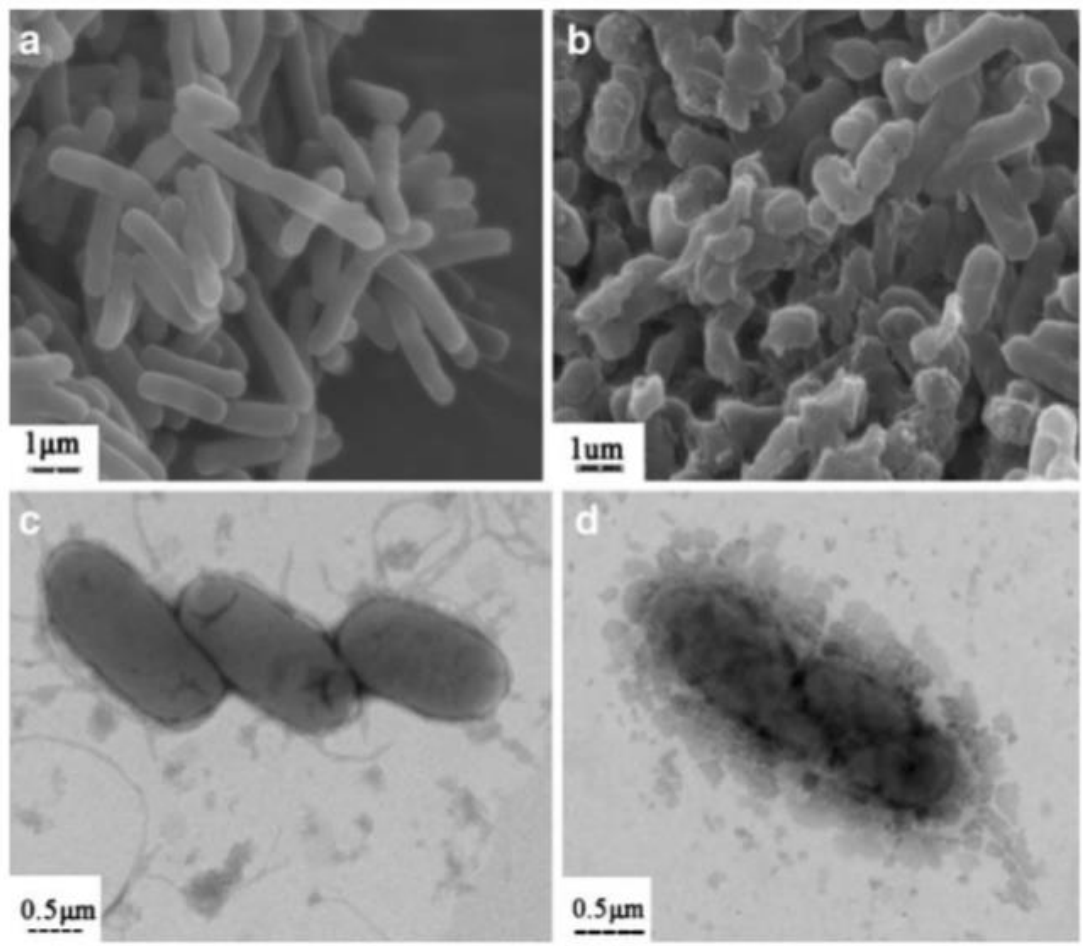

Figure 2.14. SEM (a, b) and TEM (c, d) images of native *E.coli* cells (a, c) and *E.coli* cells treated and untreated with Ag NPs [61].

2.3.3. Silver Nanoparticle (Ag NP) Loaded Nanocomposites

Ag NPs are one of the most promising nanomaterials for antimicrobial applications due to their high bactericidal effect against bacteria, fungi and low toxicity against

mammalian cells [64]. Therefore, they are frequently used as nano reinforcements in the fabrication of antibacterial, antifungal and antiviral nanocomposites [65].

2.3.3.1. Silver Nanoparticle/Polylactide (PLA) Nanocomposites

Ag NP/PLA nanocomposites were studied in order to import antibacterial activity to PLA matrix. In Shameli's study, Ag NP/PLA nanocomposite films were synthesized and antibacterial properties of the nanocomposite films as a function of Ag NP loading were investigated against *E. coli*, *Vibrio parahaemolyticus* and *Staphylococcus aureus* [17]. Disk diffusion test results showed that nanocomposite films form large inhibition zone especially against *Vibrio parahaemolyticus* and *Staphylococcus aureus (S. aureus)* due to their successive Ag ion release to agar medium. Plot showing the Ag ion release rate is provided in Figure 2.15.

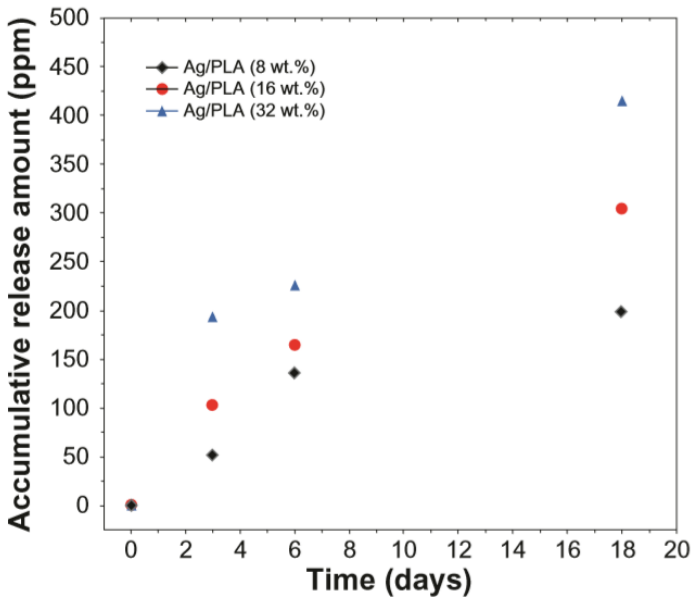

Figure 2.15. Ag ion release curves of Ag NP/PLA nanocomposites films with 8, 16, 32 wt.% Ag NP [17].

In addition, size of inhibition zones of bare PLA and nanocomposites are given in Table 2.2. In this study, addition of NPs formed a clear zone around films and this clear region get enlarged at higher Ag NP contents. Also, Ag NPs showed higher resistance to *Vibrio parahaemolyticus* and *S. aureus* mainly due to difference in cell wall structures.

Table 2.2. Inhibition zones for bare PLA and Ag NP/PLA nanocomposites films with 8, 16, 32 wt.% Ag NP [17].

Bacteria Film samples	Inhibition zone (mm)		
	Escherichia coli	*Staphylococcus aureus*	*Vibrio parahaemolyticus*
Control	–	0.67	–
Ag/PLA 8 wt%	1.43	4.00	4.00
Ag/PLA 16 wt%	2.33	8.00	8.00
Ag/PLA 32 wt%	10.33	9.33	15.00

2.3.3.2. Silver Nanoparticles/ Halloysite Nanotubes/ Graphene Nanocomposites

In the study by Yu and Zhang, sandwich-like Silver Nanoparticles/ Halloysite Nanotubes/ Graphene **(**Ag/HNTs/rGO) nanocomposite films were fabricated and antibacterial properties against Gram-positive and Gram-negative strains were determined [18].

Minimal inhibitory concentration (MIC), defined as the lowest concentration of the antibacterial agent required for the visible inhibition, was found for sandwich like nanomaterials (Ag/HNTs/rGO) and control samples (Ag, Ag/HNTs, rGO/Ag). According to the MIC results, lowest MIC indicating highest antibacterial performance was obtained in Ag/HNTs/rGO as shown in Table 2.3.

Table 2.3. MIC of nanomaterials to *E.coli* [18].

rGO	Ag	Ag/HNTs	Ag/rGO	Ag/HNTs/rGO
1024	64	32	16	2

Moreover, bacteriostatic rate test was performed to control groups and to Ag/HNTs/rGO in this study. Reproduction of *E. coli* and *S. aureus* bacterial colonies were investigated on agar plates as shown in Figure 2.16. Bacterial reproduction was found to be completely prevented by Ag/HNTs/rGO treatment.

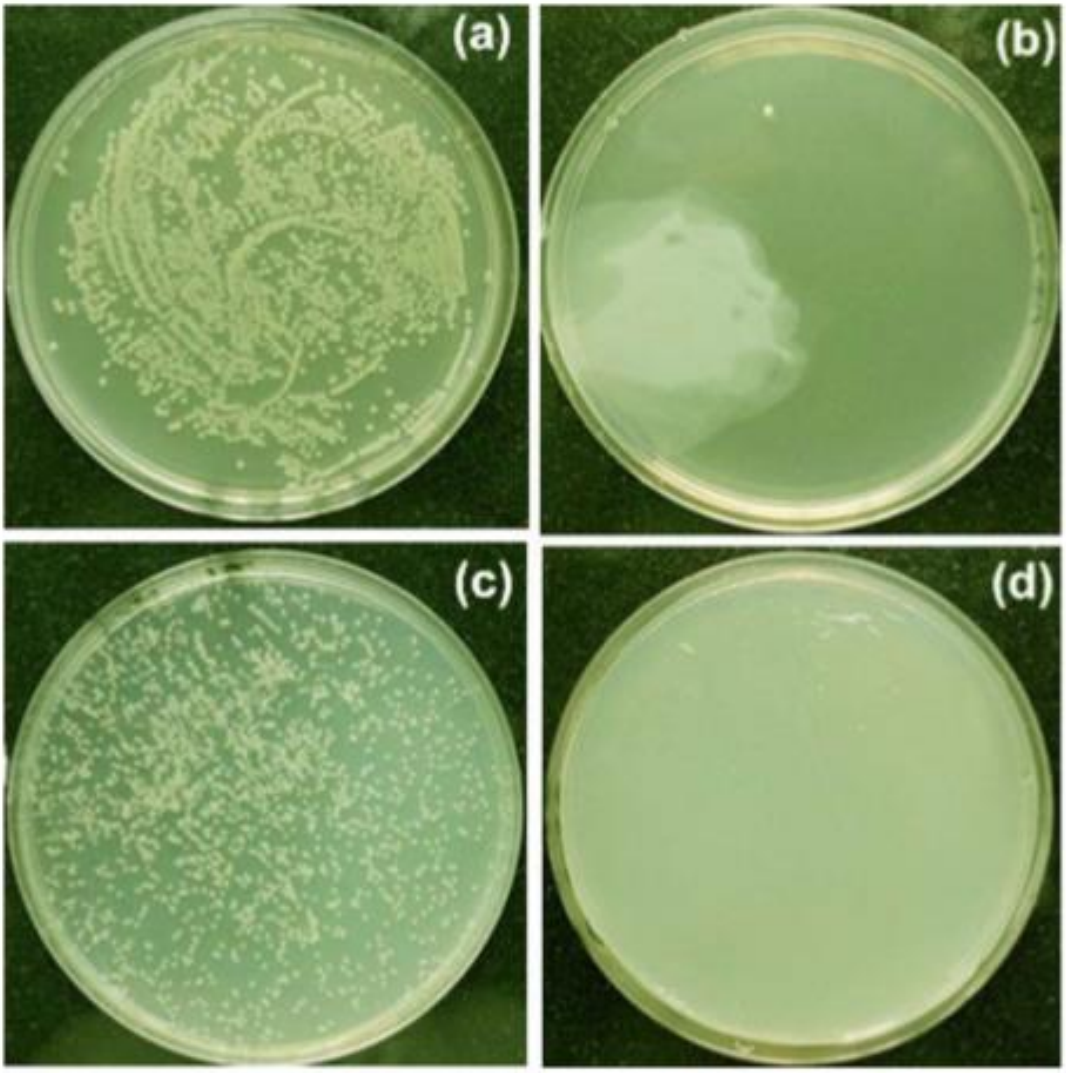

Figure 2.16. Photographs of (a, b) *E. coli* and (c, d) *S. aureus* bacterial colonies; (a, c) control groups and (b, d) treated with Ag/HNTs/rGO [18].

These results indicated that sandwich like Ag/HNTs/rGO nanocomposite films exhibited higher antibacterial performance against *E. coli* and *S. aureus* compared to Ag nanoparticles, rGO nanosheets or their nanocomposites.

2.3.3.3. Silver Nanoparticles/Chitosan

Antibacterial performances of Ag NPs were studied in a wide range of polymer matrices. In Kalaivani and coworkers study, chitosan mediated Ag NPs were synthesized and the antibacterial and antifungal activities of Ag NPs were analyzed by agar disk diffusion method [65]. Diameters of the inhibition zones against bacteria and fungi are provided in Figure 2.17 (a) and (b), respectively. Highest antibacterial activity was exhibited against *Pseudomonas* as a Gram-negative pathogen with 24 mm of inhibition, whereas highest antifungal activity was obtained against *A. niger* with 15 mm of inhibition.

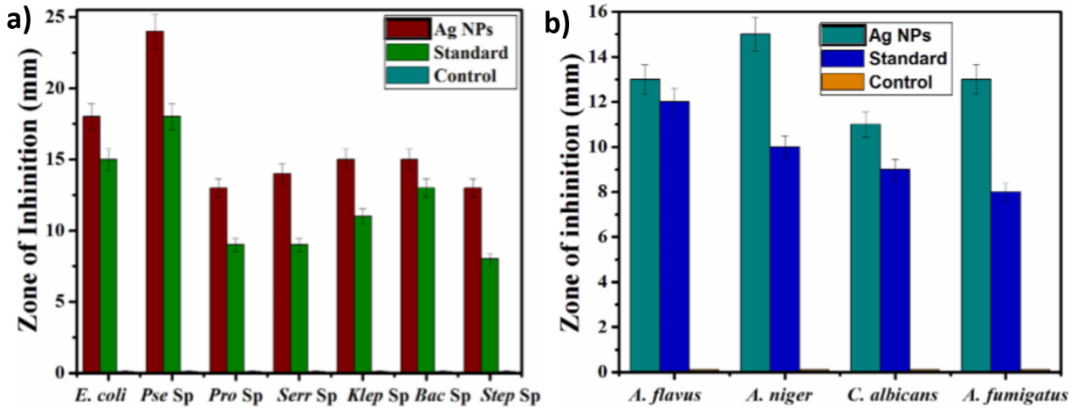

Figure 2.17. (a) Antibacterial and (b) antifungal activities of chitosan mediated Ag NPs [65].

Figure 3.1. Photographs of (a) Ag NWs dissolved in PLA/chloroform solution, (b) Ag NW/PLA nanocomposites poured into glass petri, (c) dried Ag NW/PLA pellets.**Figure 2.18.** (a) Antibacterial and (b) antifungal activities of chitosan mediated Ag NPs [65].

CHAPTER 3

EXPERIMENTAL DETAILS

3.1 Materials Used

L-lactic acid based polylactide (PLA) used in this thesis was provided by Nature Plast (PLE 001). According to the technical data sheet, PLA melts at 145-155 °C and degrades at 240-250 °C. Also, melt flow index range and density of PLA are provided as 2-8 g/10 min at 190 °C under 2.16 kg and 1.25 g/cm^3 respectively. Moreover, weight average molecular weight of PLA was found as 105800 g/mol by Gel Permation Chromatography. Poly (vinylpyrrolidone) PVP (MW=55000), ethyleneglycol (EG), silver nitride ($AgNO_3$), sodium chloride (NaCl, 99.5 %) used for Ag NWs synthesis and chloroform (99.5 %) used for the dispersion of Ag NWs were purchased from Sigma-Aldrich. All materials were used without further purification.

3.2. Ag NW Synthesis and Nanocomposite Preparation

3.2.1. Ag NW Synthesis

Ag NWs were synthesized by the polyol method, which is a solution based synthesis method, similar to the procedure reported by Coskun et al. [66]. Firstly, 80 ml of EG solution was prepared with 0.45 M PVP and 1 mM NaCl. Then, this solution was stirred at 120 °C until all the ingredients were dissolved and cooled to room temperature. At the same time, 40 ml of EG solution with 0.12 M $AgNO_3$ was prepared and stirred at room temperature. Following the preparation of solutions, $AgNO_3$/EG solution was placed in an oil bath at 120 °C. Then, PVP/EG solution was added into the $AgNO_3$ solution and oil temperature was increased to 160 °C. Solution was held there for 90 minutes.

Following synthesis, the solution was diluted with acetone and centrifuged at 7000 rpm for 10 minutes for the purification of Ag NWs. After centrifugation, Ag NWs were dispersed in chloroform. Later, NWs were separated from the by-products through decantation.

3.2.2. Preparation of Nanocomposites

PLA powders were dried at 80 °C over night under vacuum to get rid of excess moisture. Then, PLA powder was dissolved in chloroform. The prepared solution was mixed at 60 °C at 1000 rpm. Once PLA powders were completely dissolved in chloroform, desired amount of Ag NWs, previously dispersed in chloroform, were added into PLA solution. Solution was stirred at 1000 rpm until it becomes viscous. Then, the solution was poured into a glass petri and divided into small granules as presented in Figure 3.1. Finally, nanocomposites in the form of granules were dried at 60°C for 12 hours under vacuum to remove remaining solvent and moisture.

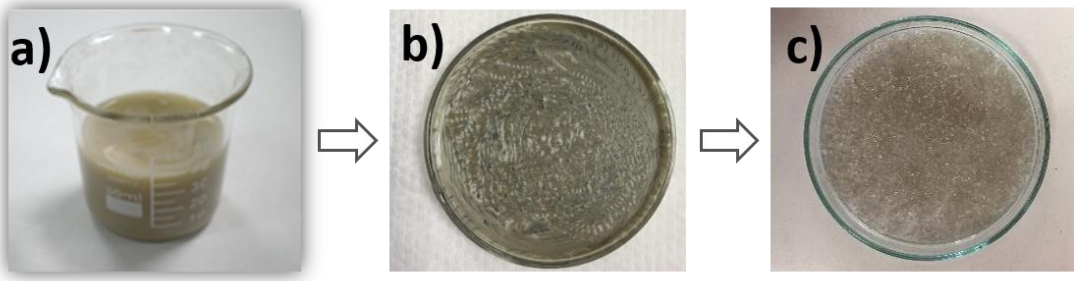

Figure 3.2. Photographs of (a) Ag NWs dissolved in PLA/chloroform solution, (b) Ag NW/PLA nanocomposites poured into glass petri, (c) dried Ag NW/PLA pellets.

3.2.3. Preparation of Ag NW/PLA Nanocomposite Filaments and 3D Printing

Ag NW/PLA nanocomposite pellets were loaded into twin screw extruder (MicroLab 400 Twin Screw) to obtain 1.75 mm filaments. Twin screw extrusion temperature profile was decided as 115, 170, 180, 175, 145 °C from feeding zone to die respectively. After then, samples to be printed were drawn in SolidWorks and ‘stl’ files were prepared. Print settings were arranged as 100% infill content, 210 °C nozzle temperature, 65 °C built plate temperature and ±45^{o} printing orientation.

Then, Ag NW/PLA filaments were printed in FDM 3D Printer (Ultimaker 2+) with a chamber size of 223x223x205 mm as shown in Figure 3.2. Finally, 3D printed samples were used for characterization and testing.

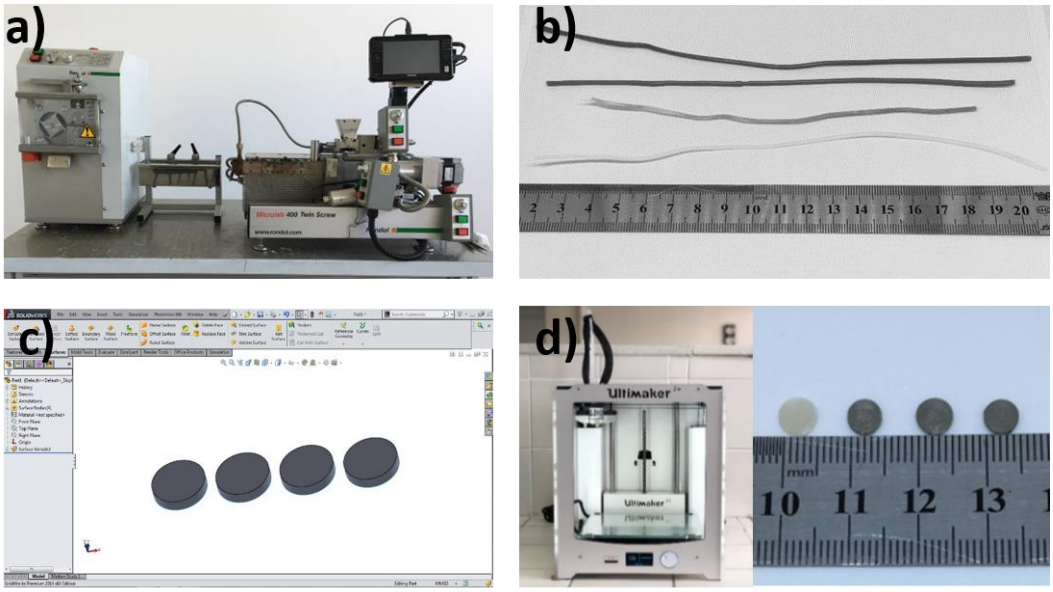

Figure 3.3. (a) Photograph of twin screw extruder used in this work. (b) Photos of Ag NW/PLA nanocomposite filaments with different Ag NW content. (c) Drawing of test sample in SolidWorks. (d) Photos of FDM 3D Printer, Ultimaker 2+ and 3D printed samples.

3.2.4. Etching

3D printed Ag NW/PLA nanocomposite disks were etched in order to get rid of polymeric film on the surface. 3D printed samples were dipped into chloroform and held there for 10 seconds. After removal of polymeric layer, samples were rinsed with deionized (DI) water to annihilate antibacterial behavior of chloroform. Finally, they were dried in a vacuum oven at 60°C over night. By this way, chloroform and water were completely eliminated.

3.3. Characterization of 3D Printed Ag NW/PLA Nanocomposites

3.3.1. Scanning Electron Microscopy (SEM)

Morphology of the printed nanocomposites and the orientation of NWs in polymer matrix was investigated by SEM (FEI Nova Nano SEM 430). Samples were coated with a thin 5-10 nm gold layer and operated under an accelerated voltage of 5 kV. To consolidate antibacterial performance evaluations, antibacterial test samples were examined again via SEM after testing. Especially, bacterial growth on the contact surface and morphology of the bacteria were investigated in detail.

3.3.2. Thermogravimetric Analysis (TGA)

In order to obtain degradation temperatures and the weight loss with temperature for solution mixed and 3D printed nanocomposites, TGA was performed via Exstar SII TG/DTA 7300 under nitrogen atmosphere. Samples were analyzed between 30 to 550 °C with a heating rate of 10 °C/min. By that way, effects of Ag NWs to PLA matrix on thermal degradation of nanocomposites were examined. To precisely determine the thermal degradation temperatures, differential thermal gravimetric analysis (DTGA) was used. Peak temperatures of DTGA curves was defined as the thermal degradation temperatures of nanocomposites.

3.3.3. Differential Scanning Calorimeter (DSC)

Crystallinity and transition temperatures of the nanocomposites were investigated by DSC analysis. Exstar X-DSC 700 system was operated under nitrogen atmosphere. Firstly, sample was heated with a heating profile from 0 to 220 °C at a heating rate of 10 °C/min and thermal history was erased. Then sample was cooled to -30 °C with a cooling rate of 10 °C/min. Then second heating was performed with the same heating profile. Crystallinity and transition temperatures were determined from the first heating of DSC curves to take previous processes into consideration for thermal characterization.

3.4. Antimicrobial Performance Evaluation

3.4.1. Disk Diffusion Test

Antimicrobial performances of 3D printed Ag NW/PLA nanocomposites against *S. aureus*, ATCC#25923 as a Gram-positive coccus, *E. coli*, ATCC#25922 as a Gram-negative basil, *Bacillus cereus* (*B. cereus*) ATCC#14603 as a Gram-positive basil and spore-forming bacteria, *Candida albicans* (*C. albicans*) ATCC#90028 as a yeast-like fungus were examined by agar disk diffusion method, adhesion capacity and time-kill assay. First of all, freshly-culturing bacterial strains of *S. aureus, E. coli and B. cereus* were prepared on Mueller Hinton agar (MHA, Merck, Germany) at 37 °C for 24-48 hours and *C. albicans* strains were cultured on Sabourraud Dextrose agar (SDA, Merck, Germany) at 37 °C for 48-72 hours aerobically. Then, grown colonies were harvested, and the bacterial and fungal suspensions were prepared in a sterilized test tube including 5 mL Mueller Hinton Broth (MHB, Merck, Germany) and the final inoculums were adjusted to 1.5 x 10^8 for bacterial strains and 2 x 10^8 for C. albicans as CFU (colony forming unit)/mL respectively according to 0.5 McFarland test standard turbidometrically and the inoculum concentrations were adjusted according to their optical density (OD_{450nm}: 0.600) spectrophotometrically, also. Then, 100 µl amount of each suspension was inoculated on the MHA for bacterial strains, SDA for *C. albicans* and the disk shaped 3D printed samples were placed onto the agar plates and aerobically incubated at 37 °C for 24-72 hours. Bacterial and fungal growth inhibition around disks were examined and the diameters of the inhibition zones were measured. In addition, bacterial survival and morphologic structures of the strains on the contact surfaces were carefully investigated by SEM. After testing, samples were held in refrigerator for 1 week and examined again.

3.4.2. Time Kill Test

3D printed nanocomposites were also tested by time-kill assay to find out their time-dependent killing capacity for application durations of 2, 4, 6, 8, 24-hours against *S. aureus* and *E. coli.* The same bacterial suspensions of these strains ($1.5x10^8$ CFU/mL concentrations), prepared for the agar disk diffusion test, were used for time-kill test under the same microbiological conditions. One milliliter Mueller Hinton Broth (MHB, Merck, Germany) medium was placed into the sterilized test tubes. Then, 3D printed samples were placed in the tubes and incubated for the selected time intervals at 37 °C. After the time-dependent incubations, the samples were taken out from the tubes and were gently washed in 1 mL phosphate-buffered solution (PBS, pH: 7.0) twice and placed into another test tube containing 1 ml sterilized distilled water, and serially diluted to (10^{-1}, 10^{-2} and 10^{-3}). Finally, 100 µl of the solution was taken out from each tube and cultured on Mueller Hinton agar plates under the same microbiological conditions overnight. Then, the freshly grown colonies were counted and calculated as CFU/mL for each test strain.

3.4.3. Adhesion Test

3D printed nanocomposites were also tested by adhesion test to clarify bacterial adhesion capacity with time on the contact surface of the disks. Same bacterial suspensions of *S. aureus* and *E. coli* were used in this assay. Following the procedures in time kill test, 20 µL of bacterial suspensions were taken out and placed onto the surfaces of 3D printed disks. Then, they were incubated for 15, 30, 60, 90 minutes under the same microbiological conditions. After incubation, test samples were washed with PBS and serially diluted (10^{-1}, 10^{-2} and 10^{-3}) with the same method. 100 µl of each diluted solution was cultured on Mueller Hinton agar plates and incubated for 24-48 hours. Finally, grown colonies were counted and calculated as CFU/mL for each strain.

3.4.4. Fixation of Microorganisms for SEM Analysis

Bacteria were fixed onto test samples before the SEM analysis to obtain bacterial morphology without any deformation caused by vacuum or voltage. Firstly, 2 vol. % glutaraldehyde/PBS buffer solution was prepared, and the samples were held for 20 minutes in that solution by following the procedure explained in literature [67]. Secondly, 60, 70, 80, 90 vol. % ethanol/PBS buffer solution and pure ethanol solutions were prepared. Samples removed from 2 vol. % glutaraldehyde/PBS buffer solution were washed for 10 minutes in each ethanol/PBS solutions with different concentrations, respectively. After removing from ethanol solution, samples were examined in detail under SEM.

CHAPTER 4

RESULTS AND DISCUSSIONS

4.1. SEM Analysis

4.1.1. Determination of Ag NW Morphology

Ag NWs were synthesized as described in the experimental section, purified by decantation method and morphologically analyzed using SEM. SEM images of as-synthesized and purified Ag NWs are given in Figure 4.1 (a) and (b). According to the figures, NWs were synthesized and dispersed in a solvent successfully without any agglomeration or contamination. NWs were approximately 7 µm in length and 60 nm in diameter.

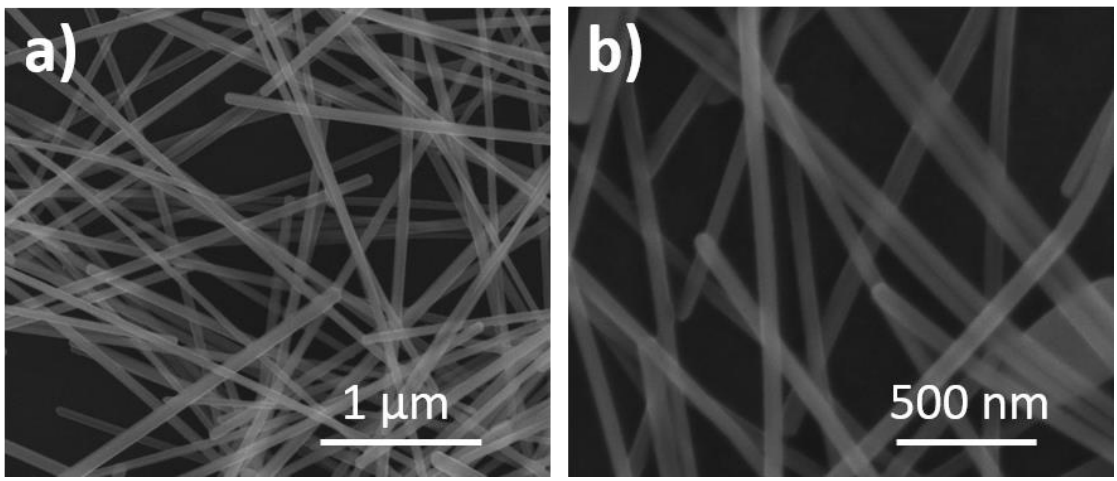

Figure 4.1. SEM images of synthesized and purified Ag NWs in (a) low and (b) high resolution.

4.1.2. Distribution of Ag NWs in PLA Matrix

4.1.2.1. Distribution of Ag NWs in PLA Matrix before 3D Printing

Ag NW loaded PLA nanocomposites were investigated under SEM to monitor the distribution of NWs in polymer matrix just after solution mixing without any extrusion processes. Figure 4.2 (a) - (d)shows the SEM images of bare PLA, 2.5, 5 and 10 wt.% Ag NW loaded PLA nanocomposite films, respectively.

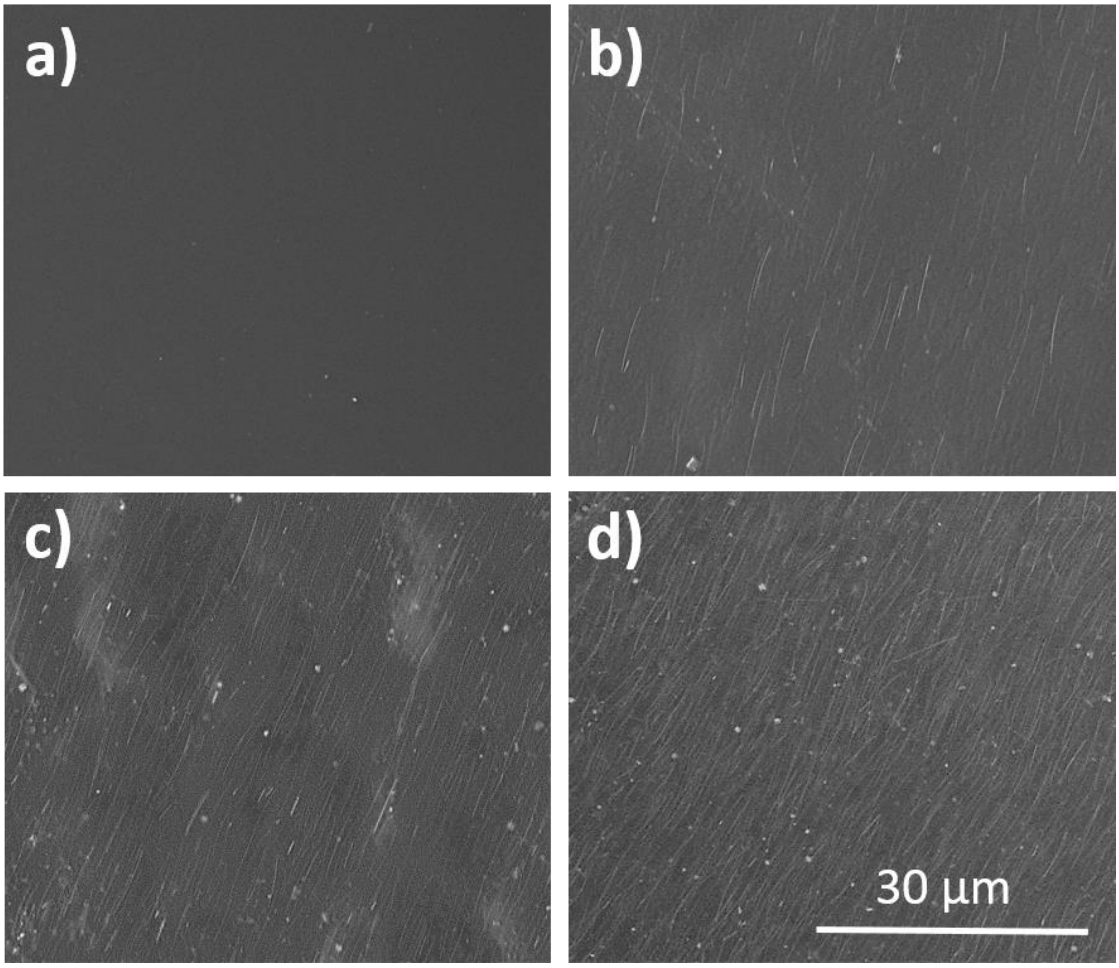

Figure 4.2. Top view SEM images of (a) solution mixed bare PLA and solution mixed nanocomposites with Ag NW loadings of (b) 2.5, (c) 5, (d) 10 wt.% before extrusion processes. All the scales are the same.

Based on these SEM images, it can be summarized that NWs were distributed homogenously in the polymer matrix. Agglomeration was totally prevented even at high Ag NW loadings due to existing PVP layer around NWs. Moreover, NWs were found to be highly aligned in the direction of the shear force. SEM images given above show that Ag NW/PLA nanocomposites were fabricated successfully by solution mixing.

On the other hand, Ag NPs were observed in the nanocomposites. This is most probably caused by the fact that purification was carried out in chloroform and NPs could not completely sink to the bottom in chloroform as in ethanol due to density difference. Therefore, complete separation of NWs and NPs cannot be achieved during purification. However, existence of NPs does not have any drawbacks in this study, as optical transparency or electrical conductivity are not the primary concerns.

4.1.2.2. Distribution of Ag NWs in PLA Matrix after 3D printing

Morphologies of Ag NW/PLA nanocomposites were also investigated following 3D printing using SEM in order to monitor the effect of extrusion process and thermal cycles on NW distribution and NW morphology. SEM images of 3D printed and etched bare PLA, and nanocomposites with 1, 2, 4 wt.% Ag NW loadings are given in Figure 4.3 (a) – (d), respectively.

Firstly, it was realized that alignment degree of NWs was decreased during extrusion mostly caused by shortening of NWs and the material started to show isotropic behavior, which is desirable especially when mechanical strength in all directions is required and inadvisable when electrical and thermal conductivity is needed. However, alignment of NWs is not a decisive parameter for antibacterial performance. Therefore, it is not of prime importance to maintain alignment of NWs for this study.

Secondly, density of NWs was decreased dramatically during extrusion process as can be clearly understood from the SEM images of 3D printed nanocomposites. High amount of Ag loss was caused by stacking of NWs with in the inner walls of the extruder.

TGA residue for the samples both before and after 3D printing helped to verify the Ag loss during extrusion. Based on these factors, initial Ag NW loadings were decided to be arranged by taking the amount of Ag loss into account.

Moreover, it can be said that NWs were broken and shorten according to the SEM images due to twin screw extrusion process. However, homogenous dispersion of NWs in polymer matrix was still conserved and no agglomeration was observed, which is significant for antibacterial performance.

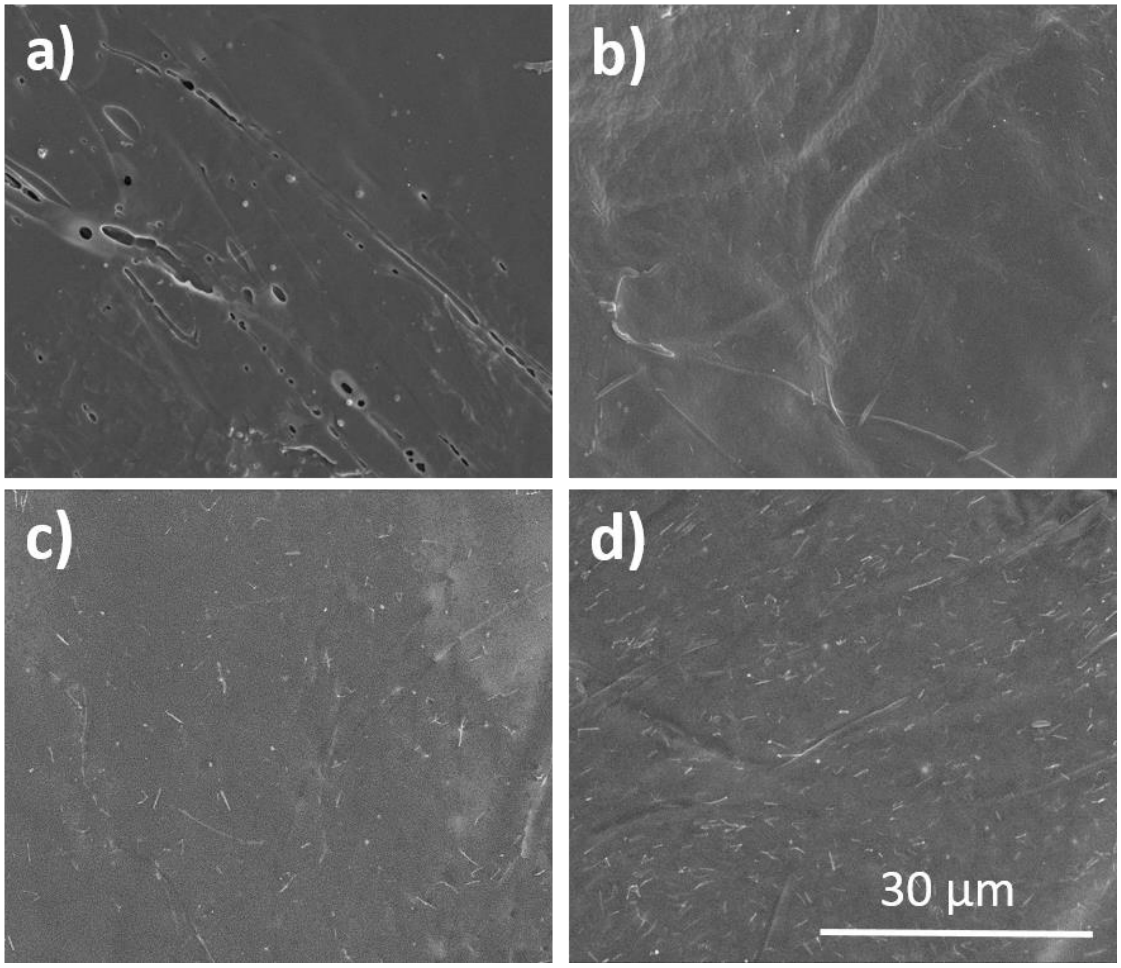

Figure 4.3. Top view SEM images of (a) 3D printed bare PLA, and 3D printed nanocomposites with Ag NW loadings of (b) 1, (c) 2, (d) 4 wt.%. All the scales are the same.

4.1.3. Effect of 3D Printing on Ag NW Morphology

In order to discuss the effects of extrusion on Ag NW morphology in detail, lengths of NWs were measured using SEM images. Figure 4.4 (a) and (b) shows SEM images of nanocomposites just after solution mixing and 3D printing, respectively.

It can be summarized that surface morphology of the NWs was protected despite of lots of thermal cycles and shear forces. However, NWs were broken into pieces and shorten to almost 1 μm length due to extrusion process, which is carried out by twin screw extruder. In twin screw extruders, material is conveyed both between the rotating screw and between the screws and the wall of the barrel [68]. This provides better mixing to produce homogenously distributed NWs in PLA matrix. However, this conveying process and shear forces deforms and breaks the NWs.

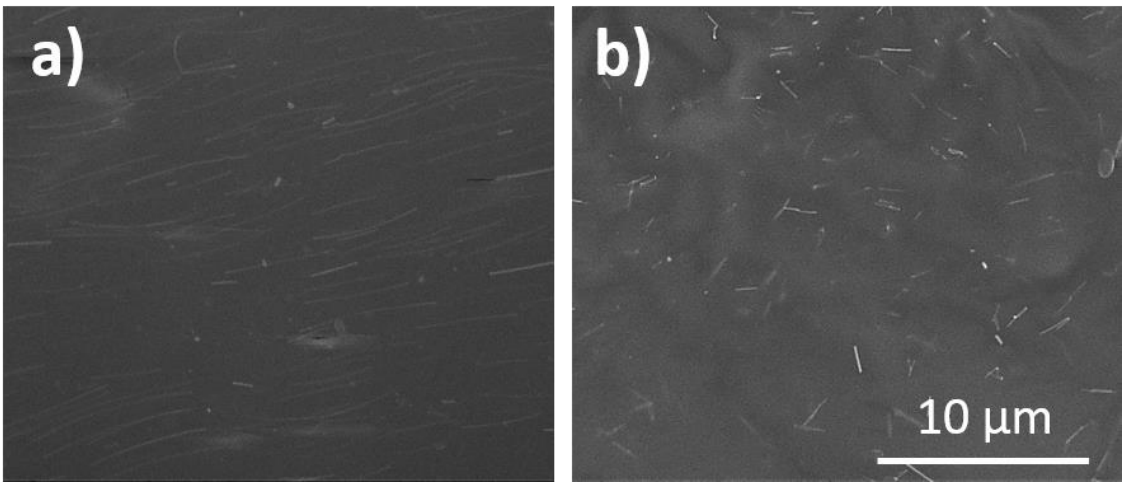

Figure 4.4. SEM images of (a) nanocomposite films right after solution mixing and (b) 3D printed nanocomposites. Both the scales are the same.

Length distribution of NWs both before and after extrusion process plotted and provided in Figure 4.5 (a) and (b). These figures summarize that NWs were approximately 7 µm long just after solution mixing, whereas they shortened down to almost 1 µm after extrusion. This also proves the fact that twin screw extrusion process breaks NWs into pieces.

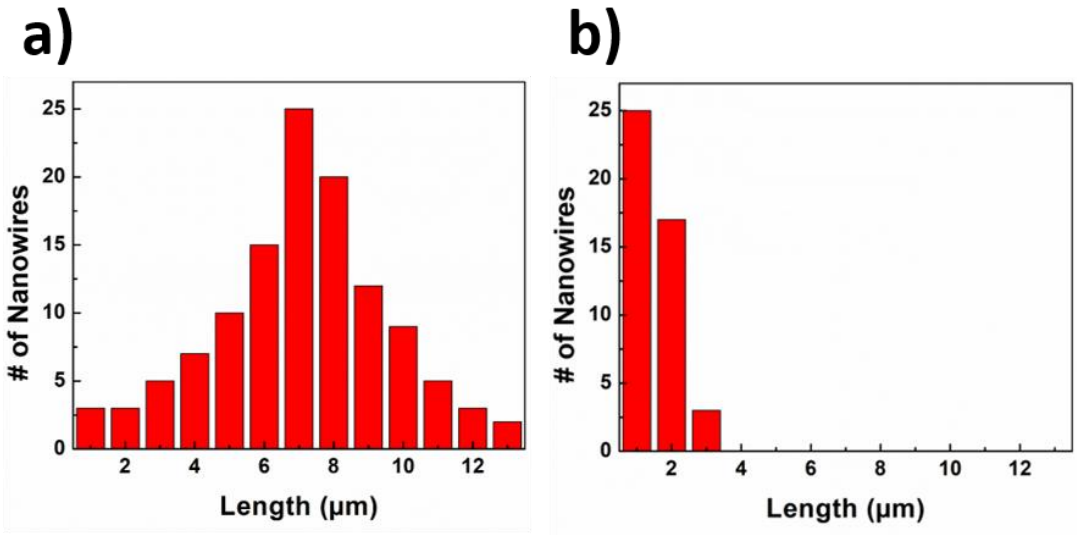

Figure 4.5. Length distribution of NWs (a) before and (b) after 3D printing.

4.1.4. Effect of Etching

Etching was carried out in order to activate NWs especially those on the surface by removing polymeric film covering 3D printed samples. Two methods were used to etch the surfaces. These were etching by microwave and etching by chloroform. Following etching, samples were examined via SEM.

Figure 4.6 shows detailed SEM images of 3D printed nanocomposites processed through microwave. It was realized based on these figures that only NWs on surface were activated and others were completely embedded into matrix. Moreover, NWs were found to be degraded, agglomerated and the NW morphology was destroyed.

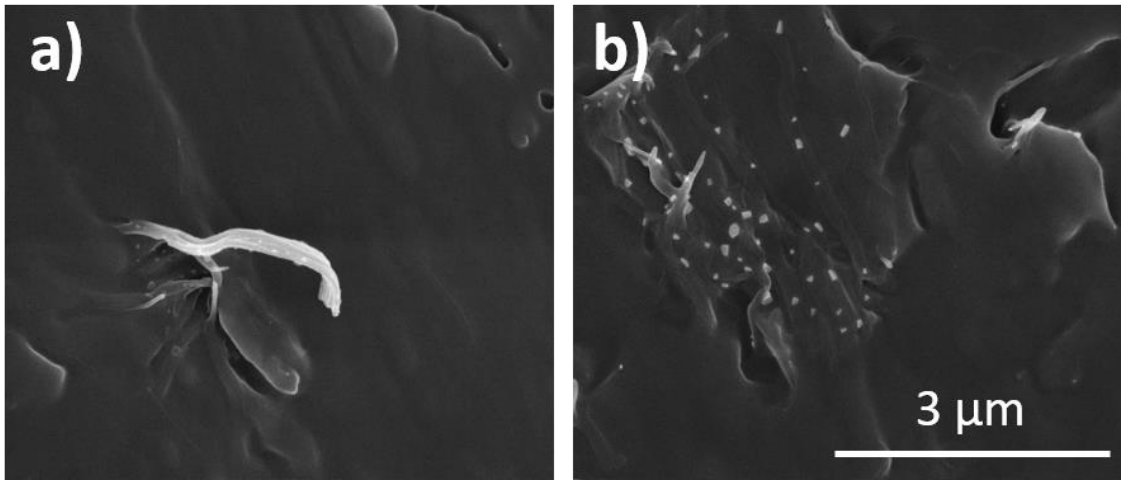

Figure 4.6. SEM images of 3D printed nanocomposites after microwave etching. Both the scales are the same.

However, both surface and embedded NWs were activated by chloroform etching as can be clearly seen in Figure 4.7. Prior to etching, very few NWs were evident within the sample whereas NWs were clarified following etching. In this treatment, it is important to optimize the etching time. It should be long enough to remove the polymer layer and short enough to avoid the degradation of the polymer matrix.

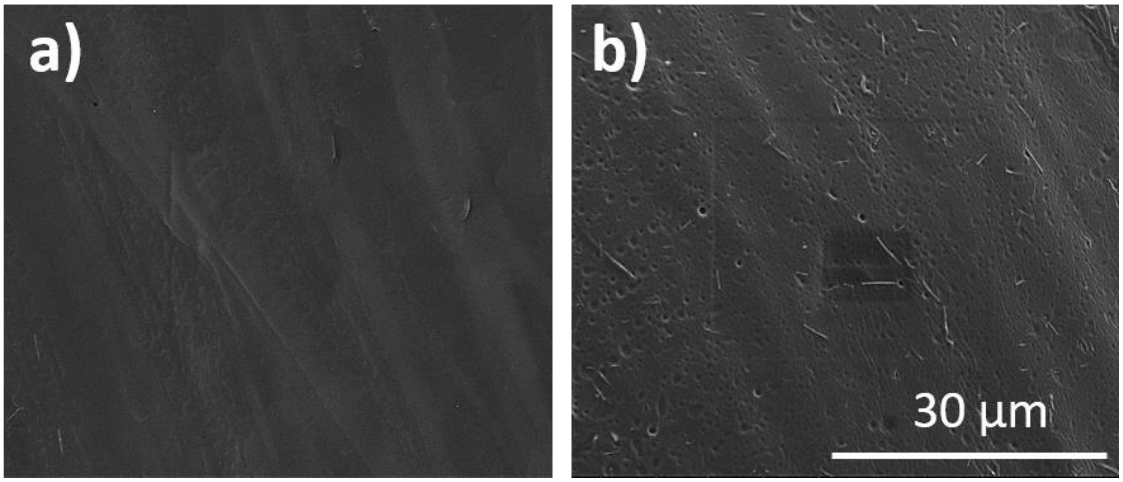

Figure 4.7. SEM images of 3D printed nanocomposites (a) before and (b) after chloroform etching. Both the scales are the same.

4.2. Thermal Analysis

4.2.1. Thermogravimetric Analysis (TGA)

TGA shows weight loss of the composites with temperature and the point where dramatic weight loss is obtained determines the degradation of the composites. TGA thermograms give general information about the degradation behavior of nanocomposites, but to precisely determine the degradation temperatures, differential thermogravimetric (DTG) graphs are plotted. Peak points of these curves represent exact degradation temperatures of the nanocomposites. Moreover, TGA gives an idea about the filler content since only Ag and inorganic ash remain at the end of test. Therefore, in this study, TGA was performed both before and after extrusion not only to discuss the effects of 3D printing on degradation behavior of nanocomposites but also to compare filler contents of the nanocomposites. This also helps to realize the Ag NW loss during twin screw extrusion and 3D printing processes.

4.2.1.1. Thermogravimetric Analysis before 3D Printing

TGA thermograms of solution mixed nanocomposites with different Ag NW loadings are provided in Figure 4.8. Solution mixed nanocomposites were in the film form and not subjected to any extrusion process. This figure implies that Ag NWs slightly influenced the degradation of polymer matrix. TGA curves slowly moved towards right with increasing Ag NW loadings.

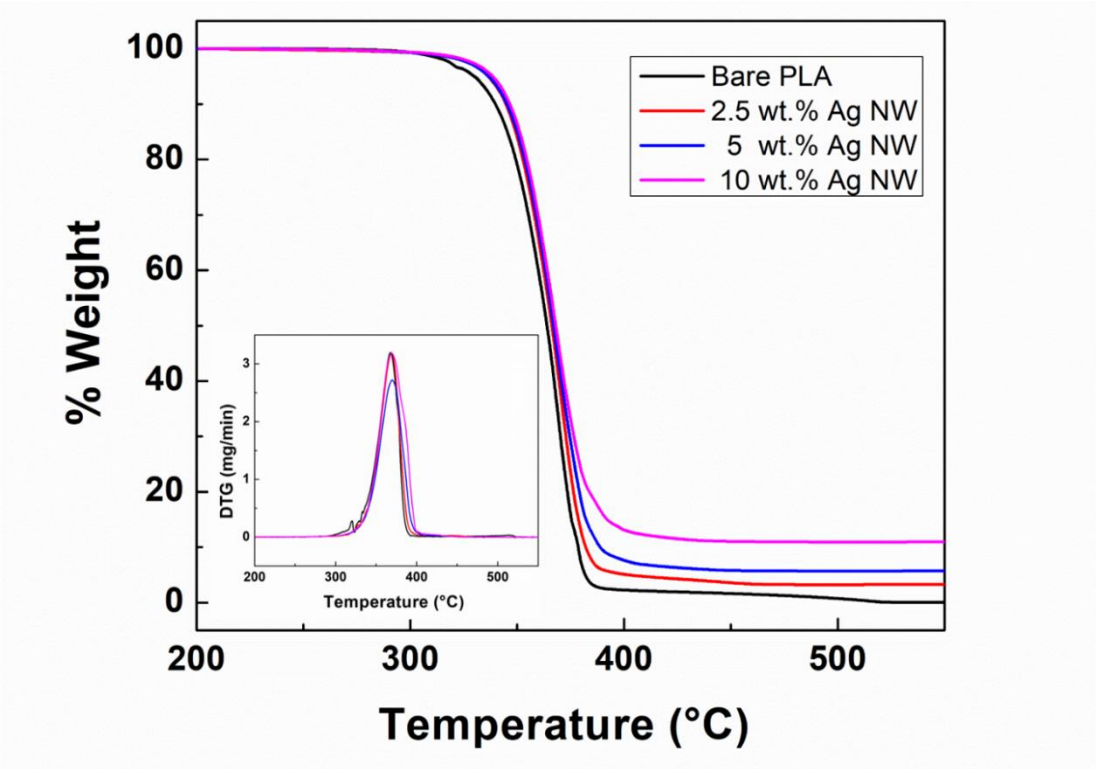

Figure 4.8. TGA thermograms of bare PLA and Ag NW/PLA nanocomposites before 3D printing. Inset shows the corresponding DTG thermograms.

4.2.1.2. Thermogravimetric Analysis after 3D Printing

TGA thermograms of twin screw extruded and 3D printed nanocomposites are given in Figure 4.9.

Firstly, % weight loss until 500 °C showed that the remaining inorganic residue is much lower than that before 3D printing. This implies that large amount of Ag NWs was lost during twin screw extrusion and 3D printing processes. Especially during twin screw extrusion, Ag NWs were stuck onto the inner walls of the extruder and so to fix percent Ag loss for all sample groups with different compositions (2.5, 5, 10 wt. %), extruder was cleaned from Ag by extruding large amounts of bare PLA in each turn. Percent Ag loss during extrusion and printing was determined as 60% by comparing the weight losses within both TGA results. Nanocomposites prepared by solution mixing with 2.5, 5, 10 wt. % Ag NW loadings were decreased to 1, 2, 4 wt. %. Secondly and most importantly, Ag NWs were found to push the degradation of matrix to higher temperatures. This is mostly caused by the dramatic decrease in the degradation temperature of bare PLA after 3D printing.

Degradation temperatures of the samples both before and after 3D printing are tabulated in Table 4.1. These results indicated that the addition of Ag NWs slightly improved thermal stability by retarding the degradation and maintained this improvement even after 3D printing. On the other hand, it was realized that the degradation temperature of bare PLA was strikingly lowered to 343 °C after 3D printing due to twin screw extrusion and 3D printing processes consistent with the previous studies [69], [70]. However, the addition of Ag NWs was found to act as a barrier to inhibit degradation of PLA matrix and to prevent decrease in degradation temperature of nanocomposites after 3D printing.

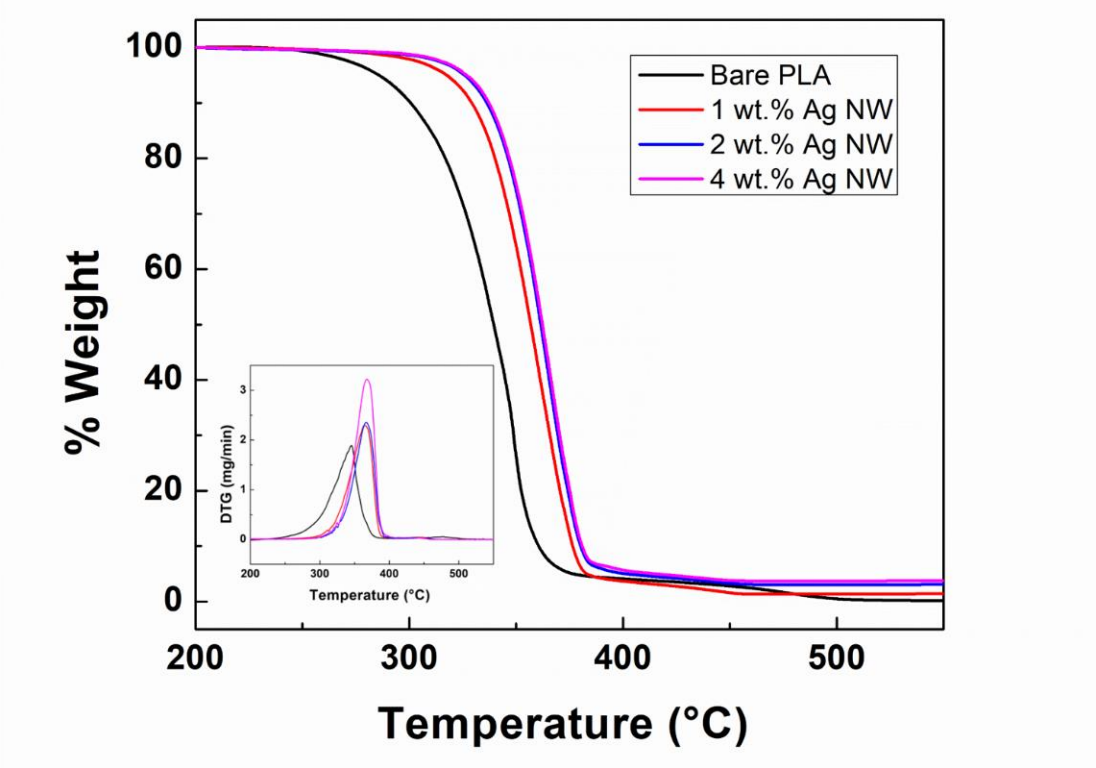

Figure 4.9. TGA thermograms of bare PLA and Ag NW/PLA nanocomposites after 3D printing. Inset shows the corresponding DTG thermograms.

SEM images of TGA residues before and after 3D printing are provided in Figure 4.10 (a) - (d). This examination was carried out in order to observe morphological changes on NWs at the end of TGA and to prove that inorganic residue was totally composed of Ag.

Firstly, SEM images of TGA residue, performed before 3D printing Figure 4.10 (a) and (b), was analyzed and it was realized that NW morphology was still conserved. Particles observed in the SEM images were probably the ones that could not be eliminated during purification of NWs. In contrast, SEM images of TGA residue after sequential extrusion processes, Figure 4.10 (c) and (d), indicated that NWs got agglomerated, shortened and turned into much bigger particles. NW morphology was completely lost due to high temperature thermal cycles.

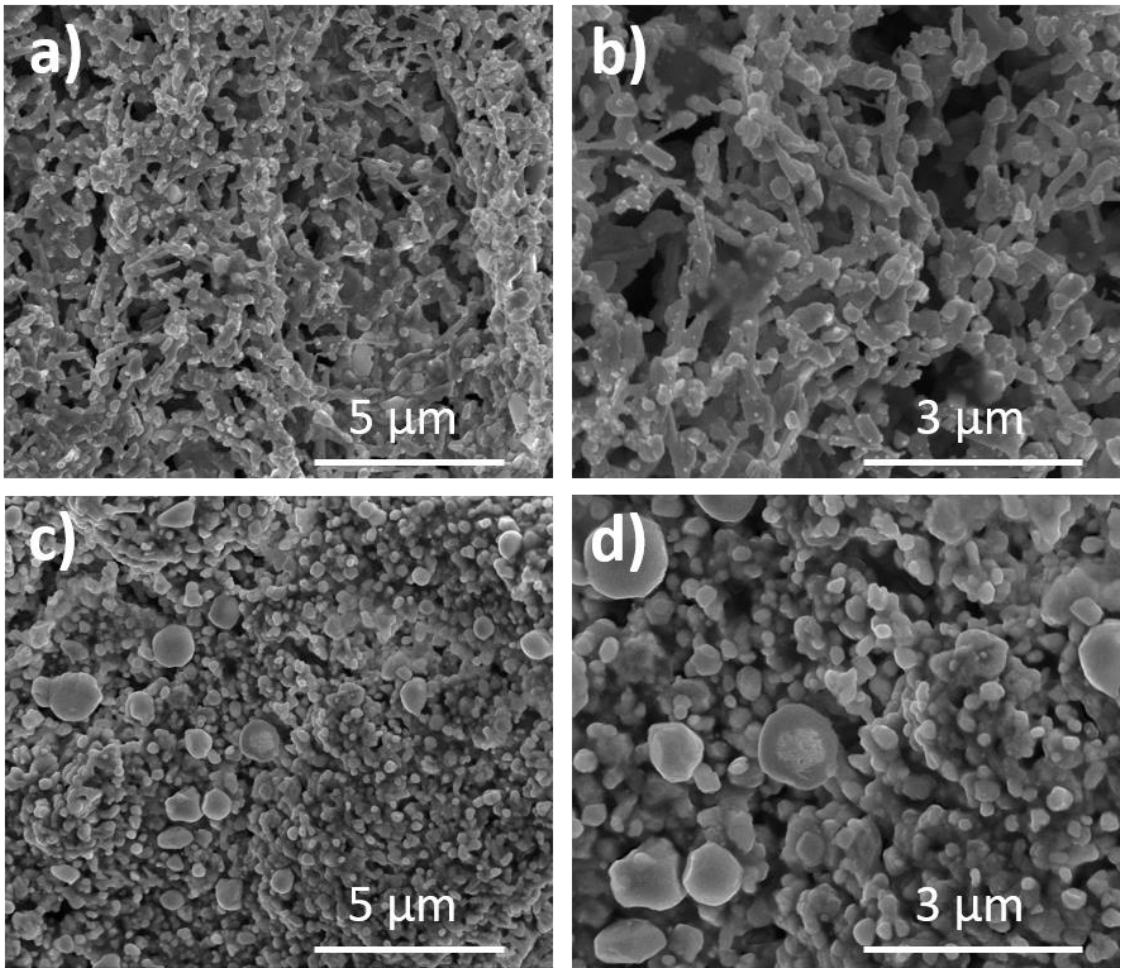

Figure 4.12. SEM images of TGA residue (a, b) before, and (c, d) after 3D printing.

4.2.2. Differential Scanning Calorimetry (DSC)

DSC is performed for the investigation of transition temperatures such as glass transition temperature, cold crystallization temperature, melting temperature and enthalpies of these transitions. Moreover, percent crystallinity of the polymer and composites is calculated by DSC results using the relation given in Equation 1, where w_{PLA} is the weight fraction of the PLA matrix and $\Delta H_m{}^o$ is the melting enthalpy of 100% crystalline PLA determined as 93 J/g.

$$X_c = \frac{\Delta H_m - \Delta H_c}{w_{PLA}\ \Delta H_m^\circ} \times 100 \qquad \text{(Equation 1)}$$

In this study, DSC was carried out before and after 3D printing to investigate the effects of Ag NWs and 3D printing on thetransition and crystallinity of the PLA matrix.

4.2.2.1. Differential Scanning Calorimetry before 3D Printing

First heating thermograms of solution mixed bare PLA and nanocomposites are provided in Figure 4.11. Firstly, it was realized that the melting temperatures of the samples remained almost unchanged with the Ag NW addition, consistent with the previous study by Doganay et al. [71]. Secondly, glass transition temperature decreased by increasing the Ag NW content as a result of poor interfacial interactions between nanowires and the polymer matrix, similar to Skorski and Esenther's study [11]. Poor interaction was resulted in increased free volume, improved polymer chain mobility, and thus lower glass transition temperatures with the addition of Ag NWs.

Thirdly and most notably, no cold crystallization peaks were observed in the first heating DSC analysis of each sample. This implies that crystalline portion of the polymer matrix got completely crystallized during solution based fabrication of the samples. Holding samples in an oven to evaporate remaining solvent at 60 °C provided mobility to the PLA chains and favored crystallization. Therefore, both bare PLA and Ag/NW PLA nanocomposites were found to show high crystallinity as expected. Percent crystallinity of bare PLA was calculated as 17% and increased with Ag NW addition up to 30% as tabulated and provided in Table 4.1. This is because, NWs acted as nucleation sites and promoted heterogeneous nucleation.

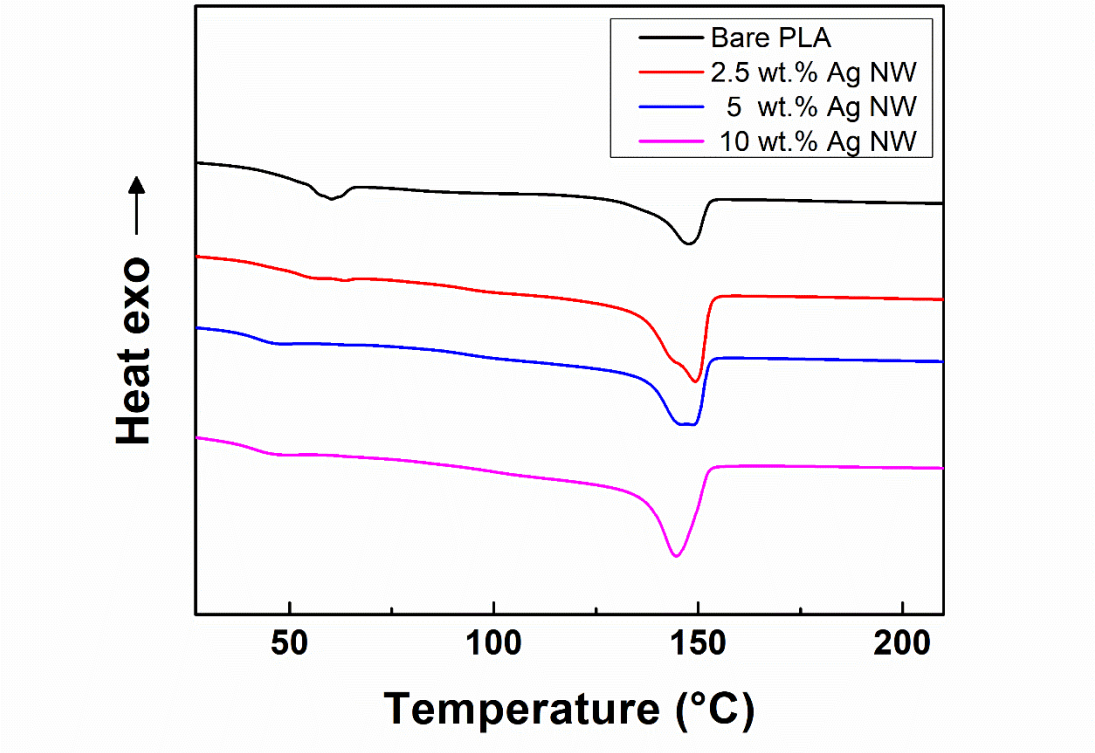

Figure 4.13. First heating DSC thermograms of bare PLA and Ag NW/PLA nanocomposites before 3D printing.

4.2.2.2. Differential Scanning Calorimetry after 3D Printing

First heating thermograms of 3D printed bare PLA and nanocomposites are provided in Figure 4.12. Transition temperatures (glass transition and melting temperatures) were obtained similarly before and after 3D printing. Crystallinity was realized to be increased after 3D printing even though Ag NW content was decreased. This is mainly caused by the fact that 3D printing parameters influences crystallization behavior of the polymer matrix as demonstrated in the previous studies [72], [73].

In this study, high nozzle temperatures (around 210 °C) provided required energy and time for PLA chains to crystallize. At the same time, build plate of printer was heated up to 80 °C and prevented rapid cooling of molten material. These two parameters induced crystallization and increased percent crystallinity of both bare PLA and Ag NW/PLA nanocomposites.

Moreover, double melting peaks were obtained in DSC analysis of both bare PLA and Ag NW/PLA nanocomposites. This situation corresponds to melting of two distinct crystal structures with different shapes and sizes that are most probably formed during thermal cycling after a slow cooling rate [74]–[76]. Lower temperature melting peaks were around 148-150 °C, whereas higher temperature melting peaks were between 160-164 °C.

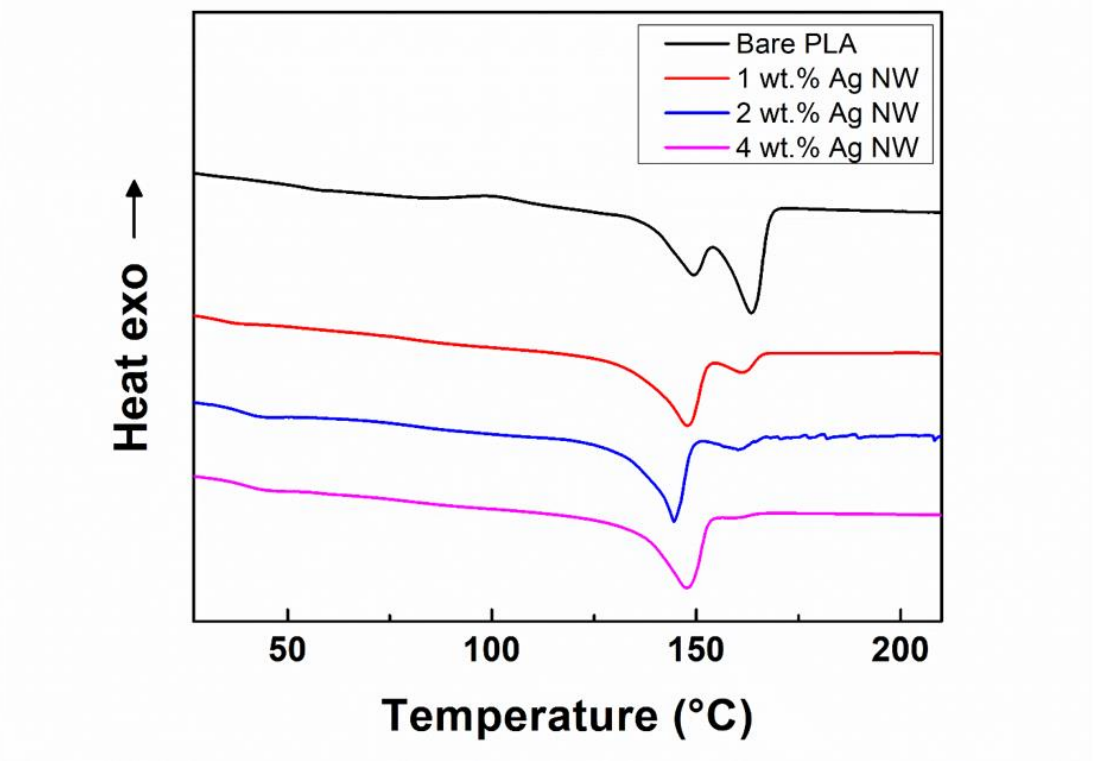

Figure 4.14. First heating DSC thermograms of bare PLA and Ag NW/PLA nanocomposites after 3D printing.

TGA and DSC results before and after 3D printing (degradation temperatures, transition temperatures, percent crystallinity) are tabulated in provided in Figure 4.1

Table 4.1. Transition temperatures and percent crystallinity of bare PLA and Ag NW/PLA nanocomposites before and after 3D printing.

Ag NW Content		**Transition Temperatures (°C)**				**% Crystallinity**
		T_d	**T_g**	**T_m**		
Before 3D Printing	Bare PLA	367	59.9	147.7		17.7
	2.5 wt. %	368	55.5	149.3		29.5
	5 wt. %	369	48.6	148.6		29.8
	10 wt. %	369	47.4	146.3		30.2
After 3D Printing	Bare PLA	343	58.7	149.6	163.6	58.2
	1 wt. %	368	35.1	148.1	161.7	38.9
	2 wt. %	369	43.9	144.3	159.9	36.5
	4 wt. %	369	44.4	147.8	161.1	42.8

4.3. Antibacterial Tests

Antibacterial tests of Ag NW loaded nanocomposites were carried out in three different ways. In this thesis, the aim is to fabricate antibacterial products that are in common daily use via simple 3D printing method. For this purpose, firstly possible application areas of 3D printed materials were specified and then, the bacterial types frequently found in these specified areas were discussed. Moreover, test methods were determined according to the application field of materials. Initially, disk diffusion method, which is the most commonly used antimicrobial performance evaluation technique was performed and then time kill essay for longer time intervals and adhesion tests for shorter time intervals were carried out. Photos of the test samples are provided in Figure 4.13.

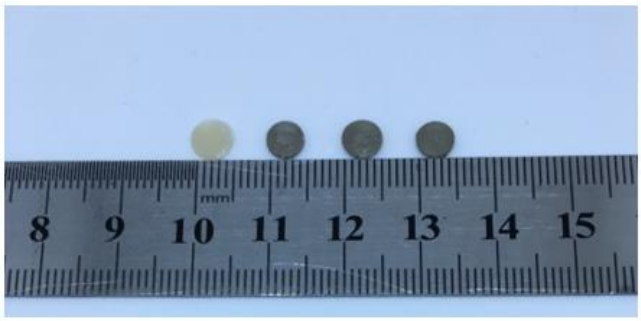

Figure 4.15. A photo of 3D printed Ag NW/PLA nanocomposites as 5 mm diameter disks with 4 different Ag NW content.

Before testing, to make sure about the purity of microorganisms, the grown colonies of the chosen microorganisms on their specific agar plates were checked, and the purity was confirmed using Gram staining and examined under an optical light microscope. Micrographs of *S. aureus*, *E. coli*, *C. albicans* and *B. cereus* are provided in Figure 4.14. Gram-positive bacteria, and as a yeast-like fungus; *C. albicans* kept their purple colour stain (crystal violet) as they cannot release this colour during decolourization stage by Gram alcohol. On the other hand, Gram-negative bacteria have an outer membrane including lipopolysaccharide molecules and they released its purple coloured stain and decolorized after the application of alcohol because alcohol has acted as a solvent and the lipid molecules of cell wall have been dissolved. Besides, the lipopolysaccharide molecules created a negative charge to the cell wall [77].

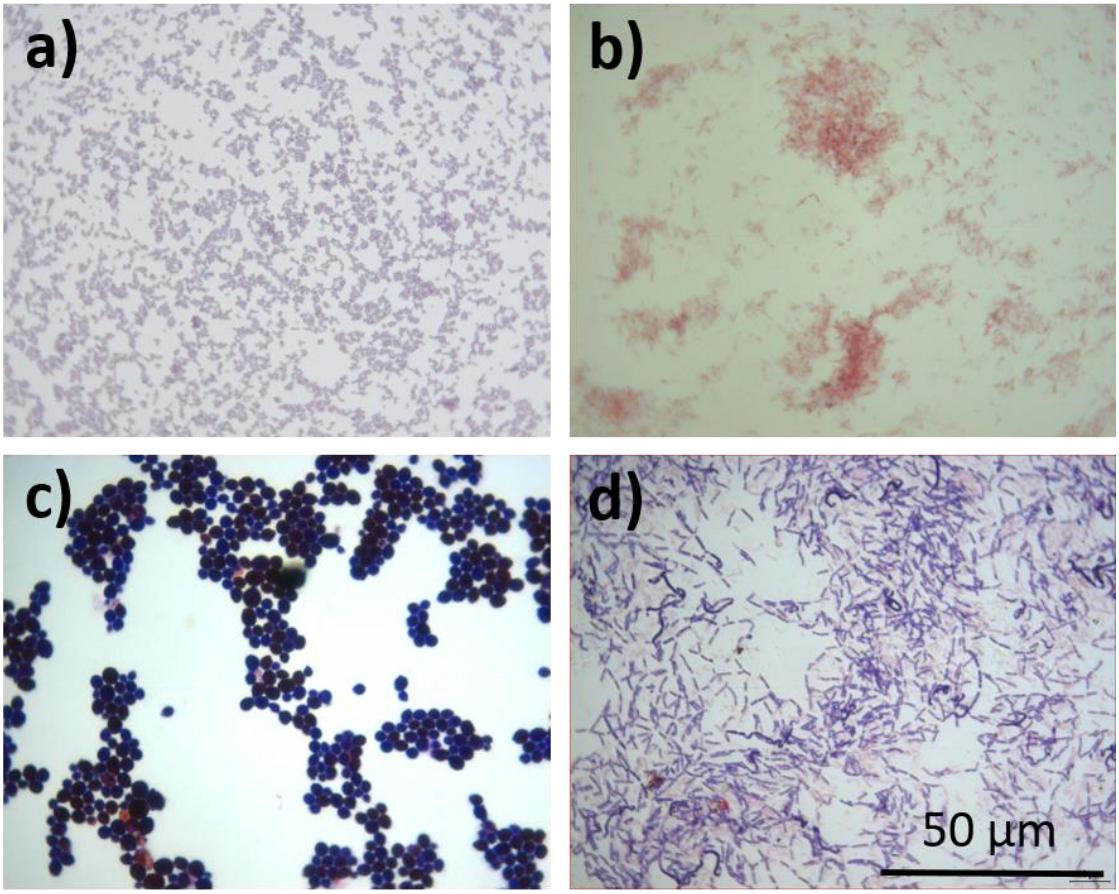

Figure 4.16. Optical micrographs of (a) *S. aureus*, (b) *E. coli*, (c) *C. albicans* and (d) *B. cereus*. All the scales are the same.

It is clear from the micrographs provided in Figure 4.14 that gram positive bacteria, which were *S. aureus*, *B. cereus* and as a yeast-like fungus *C. albicans* stained in purple colour whereas *E. coli* stained in pinkish-colour by Safranin stain as expected. Besides, it should be noted that, no contamination was observed among the microorganisms' colonies.

4.3.1. Disk Diffusion Tests

Disk diffusion tests of bare PLA and Ag NW/PLA (0.1, 0.2 and 0.4 wt.% Ag NW) were performed firstly against *S. aureus* and *E. coli.* After incubation for 24 hours, presence and size of the inhibition zones were determined around the samples, according to the photos provided in Figure 4.15.

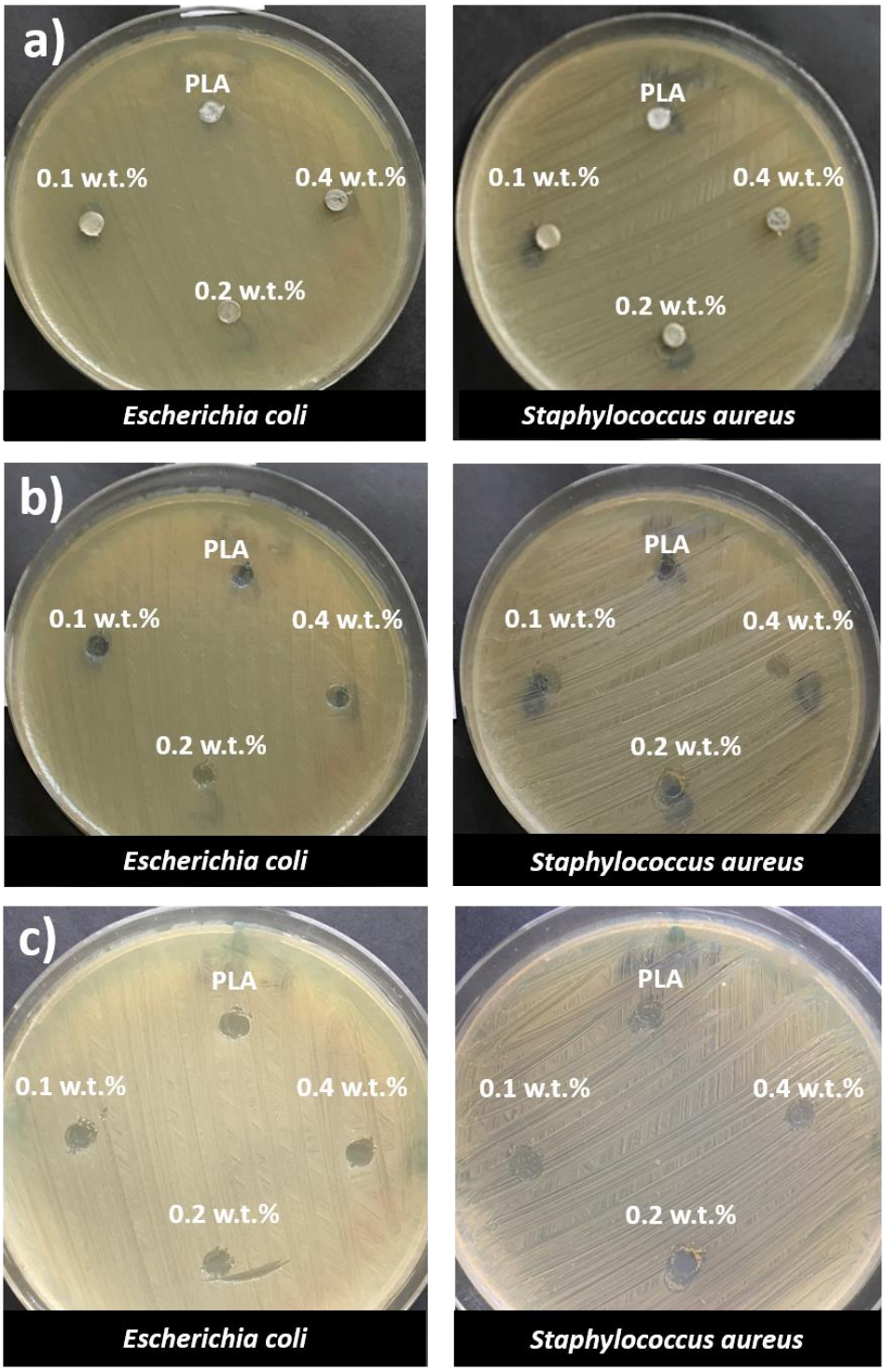

Figure 4.17. Photographs of agar disk diffusion tests of bare PLA and nanocomposites against *E.*and *S. aureus* (a) during incubation, (b) right after disk removal from medium, (c) after 1 week of incubation.

Based on these images, it is clear that no inhibition zone was formed for Ag NW based nanocomposites even for the highest Ag NW loading against both *E. coli* and *S. aureus*. This means that NWs were not well diffused into the medium, instead they were embedded into the polymer matrix. However, when disks were removed from the medium, it was observed that the bacterial growth stopped at the contact surfaces of nanocomposite disks especially on 0.4 wt.% Ag NW/PLA nanocomposite disks under the microscopic examination. After 1 week of incubation, contact surfaces were examined again and no bacterial growth were detected for both Gram-positive (*S. aureus*) and Gram-negative *(E. coli)* bacteria. In addition to *S. aureus* and *E.coli* bacteria, nanocomposites were also tested against *B. cereus* and *C. albicans* and similar results were obtained. Following testing, contact surfaces of disks were examined via SEM in order to clarify microscale inhibition of bacterial growth on the disk surface.

Based on the SEM images provided in Figure 4.16, it is summarized that notable inhibition on the bacterial growth for all cases were achieved on contact surface of the disks. Firstly, *S. aureus*, as the most frequently found bacteria on the dermal contacting sides in public areas, was examined under SEM and observed that addition of Ag NWs inhibited bacterial growth successfully only at a loading of 0.4 wt.% Ag NW. Additionally, for *B. cereus* and *C. albicans*, SEM images show that Ag ions showed antibacterial performance and inhibited bacterial growth where it contacts.

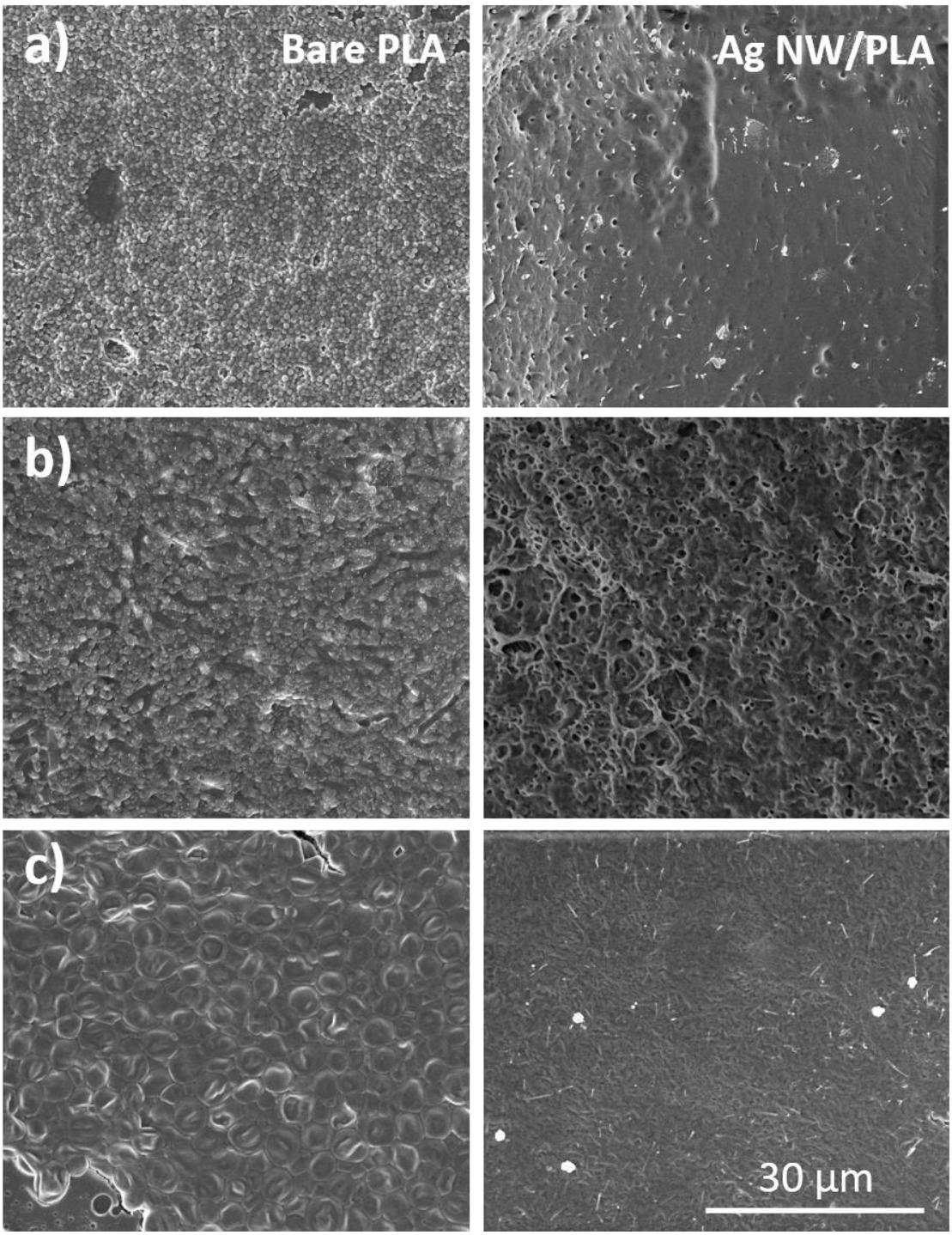

Figure 4.18. SEM images of Bare PLA and 0.4 wt.% Ag NW /PLA nanocomposites after testing against (a) *S. aureus,* (b) *B. cereus* and (c) *C. albicans.* All the scales are the same.

Moreover, not only dramatic decrease in the bacterial growth with Ag NW addition but also formation of spores were the signals of antibacterial efficacy also as they transformed into sporulation under inefficient environmental conditions. Especially, in the SEM image of nanocomposites tested against *B. cereus*, which is a Gram-positive spore forming bacteria, spore-formation was clearly obtained as shown in the SEM image provided in Figure 4.17. This implies that the environmental conditions were not suitable for that bacteria. This is because of the fact that bacterial forms are turned into spore form called sporulation to survive in inefficient environmental conditions until the conditions are restored. In this period, bacterial growth stops; but, they stay alive and wait for the favorable conditions [78]. This also proves that Ag ions destroy the environmental suitability because of its ionic exchange.

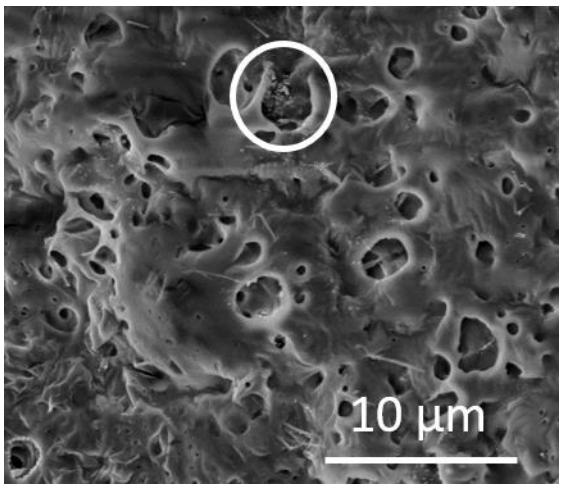

Figure 4.19. SEM images of 0.4 wt.% Ag NW /PLA nanocomposites tested against *B. cereus*.

These macro and micro examinations implied that Ag NW based PLA nanocomposites inhibited bacterial growth on their contact surface against *S. aureus*, *E. coli*, *B. Cereus* and *C. albicans* with the small amount of Ag addition (0.4 wt. %) and kept their antibacterial activity at least for 1 week. However, no inhibition zone around the disks was detected. NWs were embedded into the polymer matrix and Ag ions could not diffuse to the agar medium and thus no changes in an inhibition zone was observed. The results reported so far are not satisfactory to prove antibacterial performance of the 3D printed Ag NW based PLA nanocomposites. Based on the disk diffusion test results, it was decided that the amount of Ag NWs should be increased and surface of the disks should be etched to activate embedded NWs. Moreover, it was stated that 3D printed Ag NW based PLA nanocomposites should be tested by time kill assay to find out time dependent killing capacity of Ag NWs and adhesion tests to evaluate the bacterial adhesion capacity on the contact surface of the disks against *S. aureus* representing Gram-positive bacteria and, *E. coli* representing Gram-negative bacteria.

4.3.2. Time-Kill Assay

Time kill tests were carried out against *S. aureus* and *E. coli*. Bacterial suspensions were prepared in test tubes and samples were placed inside the tubes. Then, they were incubated (Figure 4.18) at 37 °C for different incubation periods.

Figure 4.20. Photograph of time kill test samples in incubator.

4.3.2.1. Time-Kill Assay Against *Staphylococcus aureus*

Time-kill test results against *S. aureus* are provided in Figure 4.19 for all test groups separately. Death rate (%) was calculated from the initial and final bacterial concentrations after 2, 4, 6, 8, 24 hours of incubation time and death rate versus time graph was prepared. This plot firstly shows that the addition of Ag NWs imparted antibacterial property to bare PLA. Nanocomposites with only 1 wt.% Ag NWs killed 100% of *S.aureus* up to 4 hours, which is a considerable performance only with a loading of 1 wt. % when compared to the literature [17]. Moreover, it was realized that higher Ag NW loadings resulted in longer time intervals with 100 % killing capacity. Nanocomposites loaded with 2, 4 wt.% Ag NWs killed 100 % of *S. aureus* for 8 hours. After 8 hours, antibacterial effect of NWs disappeared as a result of decreased silver ion release rate [79].

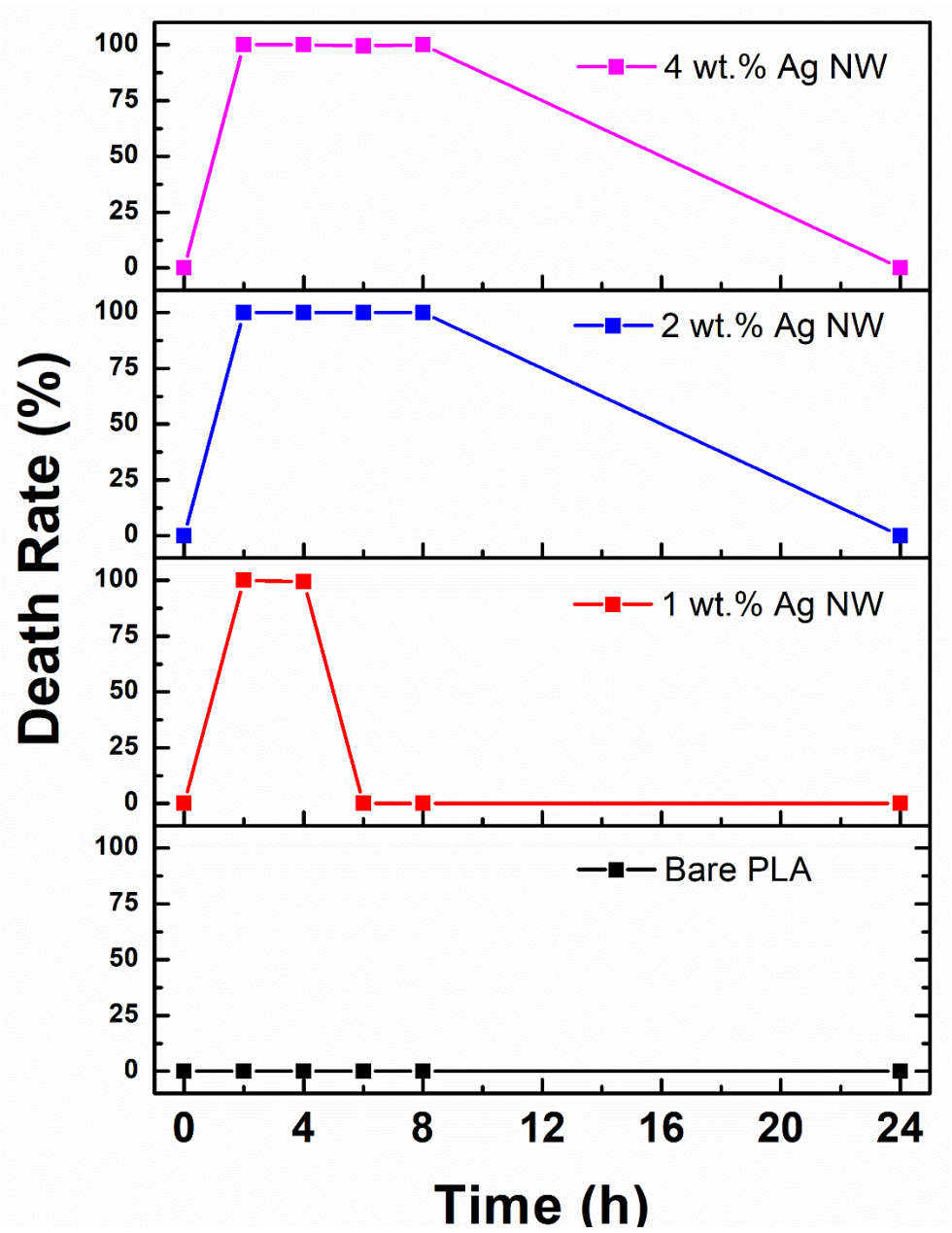

Figure 4.21. Death rate (%) with time (h) graph of time kill assay carried out for 2, 4, 6, 8, 24 hours against *S. aureus*.

Samples were examined via SEM after testing to investigate the morphologies of both dead and live bacteria. In the SEM images of 4 wt. % Ag NW/PLA nanocomposites tested for 8 hours provided in Figure 4.20 (a), damaged *S. aureus* colonies were observed as marked by red. Their morphologies were degraded and just a little amount of viable bacteria was found as marked by white. This micro examination also confirmed the time kill test results and revealed 100% killing capacity of NWs up to 8 hours.

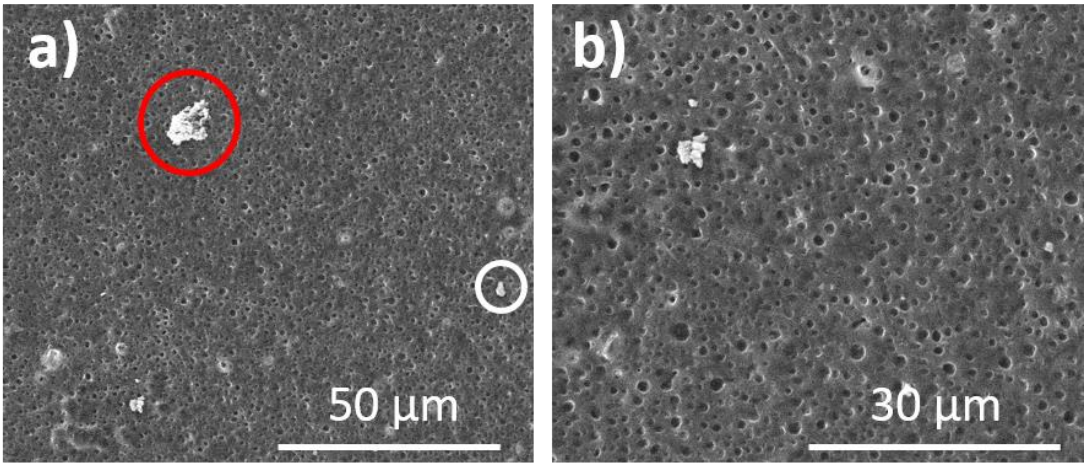

Figure 4.22. SEM images of growing *S. aureus* bacteria after 8 hours of testing with 4 wt. % Ag NW/PLA nanocomposite disks.

Photographs of incubated bacterial colonies of bare PLA and 4 wt. % Ag NW/PLA nanocomposite disks on agar plates after 8 hours of testing provided in Figure 4.21 also verified that bactericidal effects of NWs got lost after 8 hours.

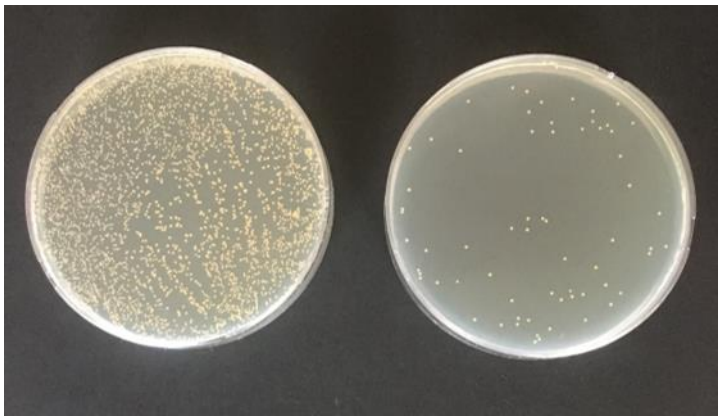

Figure 4. 23. Photograph of incubated *S. aureus* colonies in agar plates after 8 hours of testing using bare PLA (left) and 4 wt. % Ag NW/PLA (right).

4.3.2.2. Time-Kill Assay Against *Escherichia coli*

Time-kill assay results against *E. coli* are provided in Figure 4.22. This graph primarily shows that Ag NWs were much more effective to kill *E. coli* as a Gram-negative bacillus rather than *S. aureus* as a Gram-positive coccus.

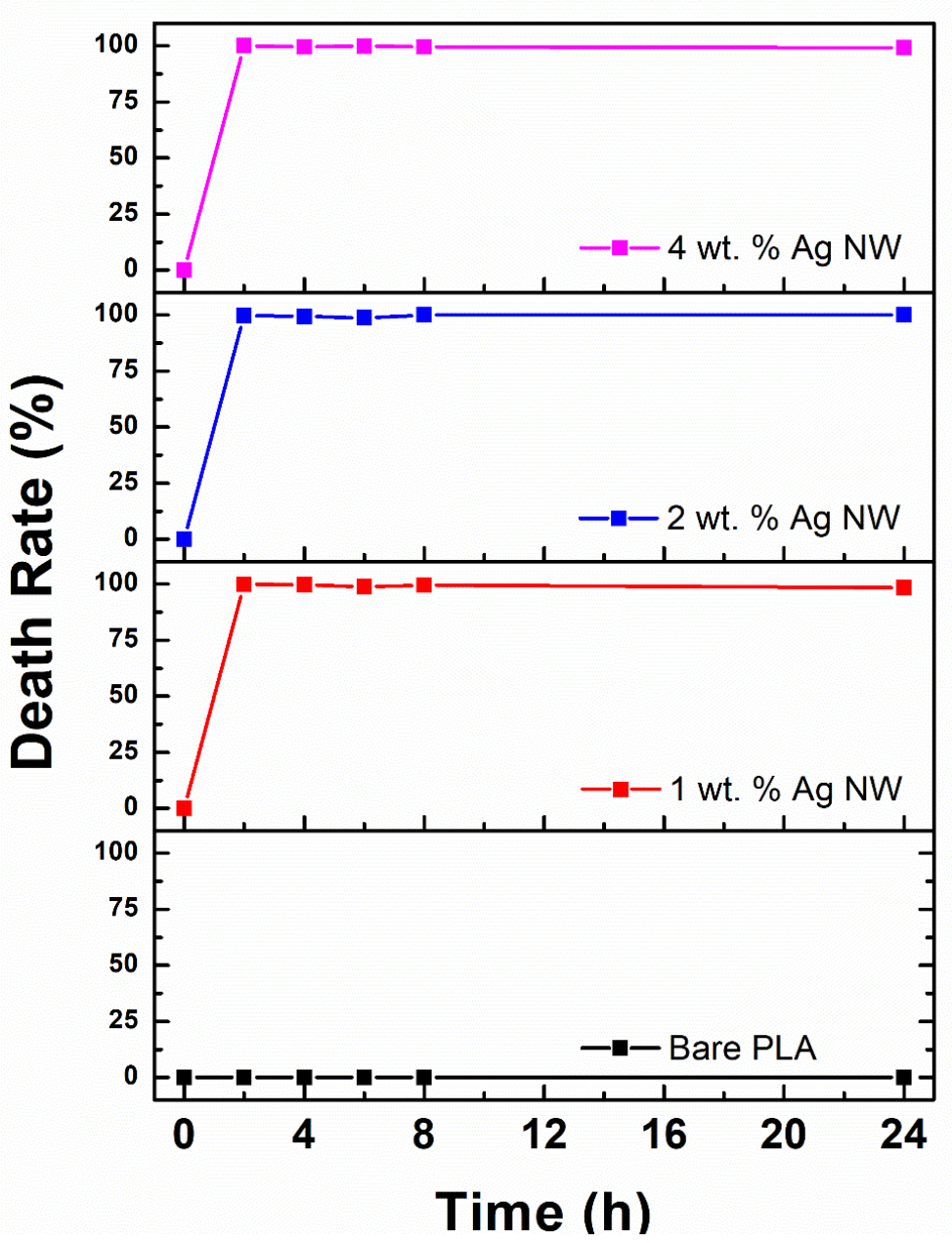

Figure 4.26. Death rate (%) with time (h) graph of time kill assay carried out for 2, 4, 6, 8, 24 hours against *E. coli*.

This phenomenon is mainly caused by the difference in cell wall structures of Gram-negative and Gram-positive bacteria. Gram-negative bacteria cells have outer membrane, thin peptidoglycan (3-4 nanometers) and cell membrane whereas Gram-positive bacteria cells are surrounded by a thicker peptidoglycan layer (30-100 nanometers). This layer, a three dimensional rigid structure composed of linear polysaccharide chains cross linked by short peptides, locks Ag ions onto the cell wall and prevents them to penetrate inside the cell [80]. In contrast, negative charge of lipopolysaccharides in the Gram-negative cell membrane supports Ag ions to adhere on cell and increases effectiveness of Ag on this type of bacteria [81]–[83]. The permeability of Ag ions into the cell wall damages protein molecules and break double stranded DNA molecules, which results in cell death. Therefore, it is an expected result for Ag NWs to show higher antibacterial performance against *E. coli* than *S. aureus* with an equal amount of Ag addition.

Moreover, when these results were analysed in detail, improved antibacterial efficiency against *E. coli* for 24 hours, longer than *S. aureus* even low amount of Ag NWs was observed. All of the Ag NW loaded samples (1, 2, 4 wt. %) killed 100% of *E. coli* just after 2 hours of incubation and did not lose their effectiveness even after 24 hours of incubation.

SEM images provided in Figure 4.23 shows dead bacteria colonies on the sample surfaces after 2 hours of incubation. This micro examination also proves the killing capacity of NWs against *E. coli.* Based on these results it is predicted that Ag NWs are more likely to penetrate Gram-negative cell wall and show higher antibacterial performance with respect to Gram-positive bacteria.

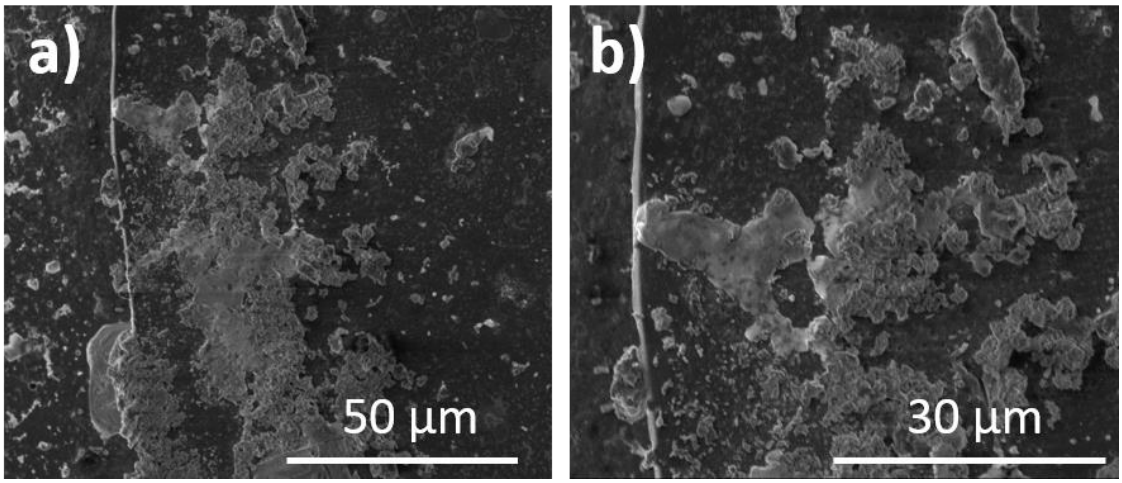

Figure 4.27. SEM images of dead *E. coli* bacteria after 2 hours of testing with 4 wt. % Ag NW/PLA nanocomposite disks.

Photographs of incubated bacterial colonies from cultivated suspensions of bare PLA and 4 wt. % Ag NW/PLA nanocomposite disks on agar plates after 2 hours of testing are provided in Figure 4.24. This figure shows that bacterial colonies were grown densely on agar that belongs to bare PLA, whereas no bacterial colony was found in the agar that belongs to Ag NW/PLA nanocomposites. It means that the addition of Ag NWs completely eliminated bacterial growth and killed 100% of *E. coli* in a short time. It can be summarized that, nanocomposites gain strong and long lasting antibacterial activity against *E. coli*.

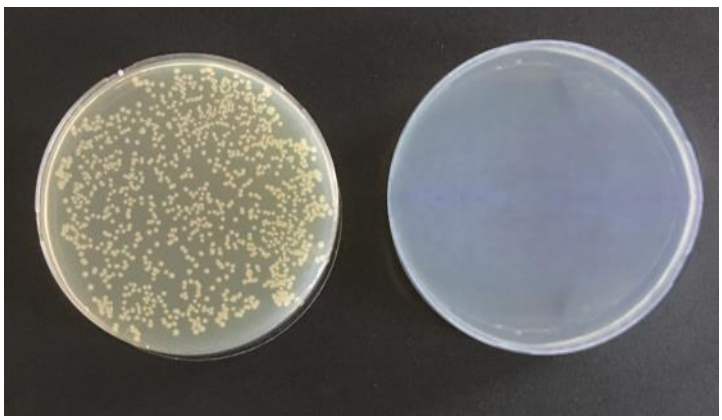

Figure 4.30. Photograph of incubated *Escherichia coli* colonies in agar plates after 2 hours of testing with bare PLA (left) and 4 wt. % Ag NW/PLA (right).

4.3.3. Adhesion Tests

Adhesion tests were carried out against *S. aureus* and *E. coli*, also. Bacterial suspensions were prepared as explained in the experimental section and 20 µL of solution was transferred to the top of the disks as demonstrated in Figure 4.25 and incubated at 37 °C aerobically.

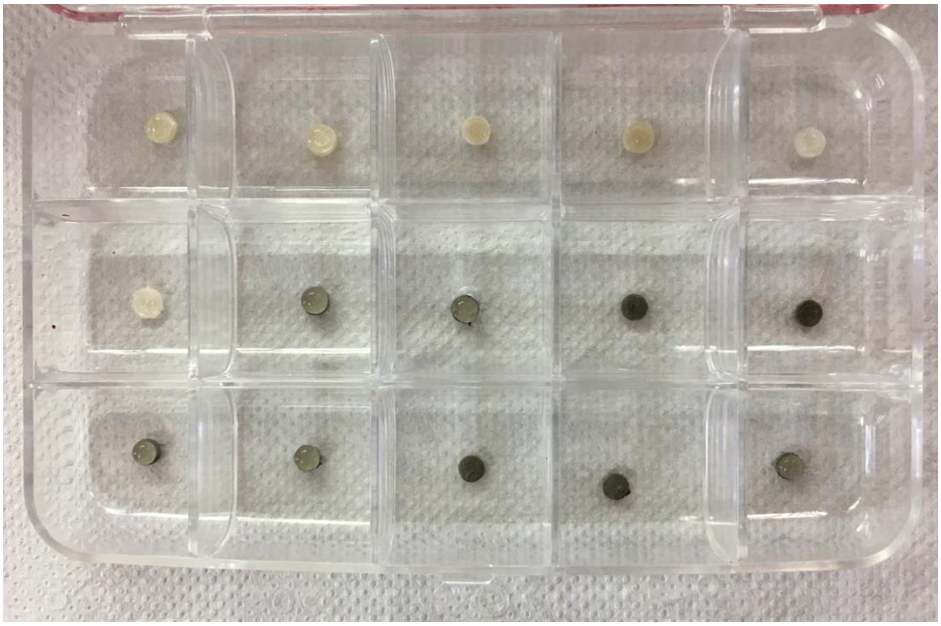

Figure 4.31. A photograph of adhesion test samples just before incubation.

At the end of the test, final bacterial concentrations were calculated. Then, bacterial concentration (CFU/mL) versus time graphs were prepared in logarithmic scale in order to indicate the changes in bacterial concentrations more precisely. Bacterial concentrations gave the number of bacteria held on the disk surfaces.

4.3.3.1. Adhesion Test Against *Staphylococcus aureus*

Adhesion test results against *S. aureus* are provided in Figure 4.26. This graph firstly shows that the bacterial concentration on the surface of bare PLA decreased from 10^8 to 10^6 CFU/mL in the first 15 minutes and then slightly changed for the next 90 minutes although it has no antibacterial behaviour. This situation is caused by the fact that all of the transferred bacteria could not be held on the sample surface most probably due to vibrations during incubation and outflow of the solution. Moreover, slight changes in the bacterial concentration on bare PLA with time can be explained by the roughness of 3D printed samples, which can directly influence the adherence ability. Also, this fluctuation between $1x10^6$ and $3x10^6$ can be a result of minor counting mistakes as they were diluted by 10^3 times for easier count. Therefore, bacterial concentration of bare PLA was used as the reference instead of initial concentration (10^8 CFU/mL) to investigate the antibacterial effect of Ag NWs.

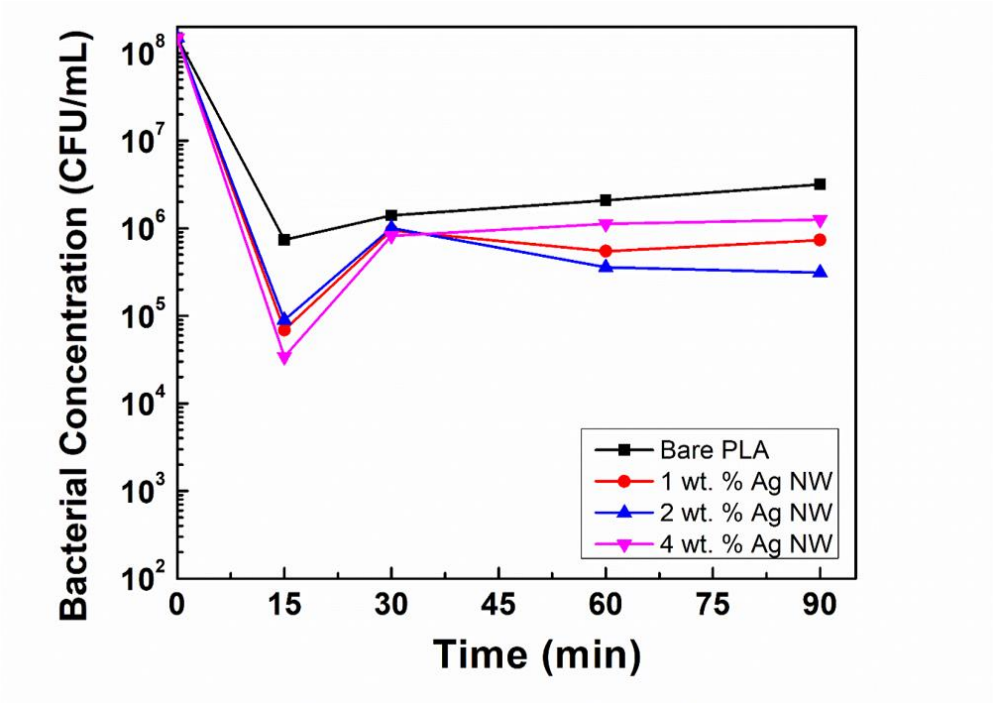

Figure 4.32. Change in bacterial concentration (CFU/mL) with time (min) after 15, 30, 60, 90 minutes of adhesion against *S. aureus.*

Secondly, 4 wt. % of Ag NWs decreased bacterial concentration to $3x10^4$ after 15 minutes of incubation. Also, similar antibacterial performance was obtained for lower Ag additions. However, it was realised that the bacterial concentrations held on the surfaces of the nanocomposites start to increase with time. It was an expected result due to high resistivity of *S. aureus* cell wall to Ag ions. Ag ions got released fast, prevented the bacteria to hold on the surface and thus inhibited their grow. However after a while, Ag ions got leached slower due to the depletion of Ag NWs, consistent with the previous studies [79] and effectiveness of the NWs decreased with time.

SEM images of the samples after 15 minutes of adhesion are provided in Figure 4.27. In this microstructure, sparse dispersion of viable and re-growing bacteria were observed as circled with white, as well as morphologically damaged bacteria cells as circled with red, proportional to the test results.

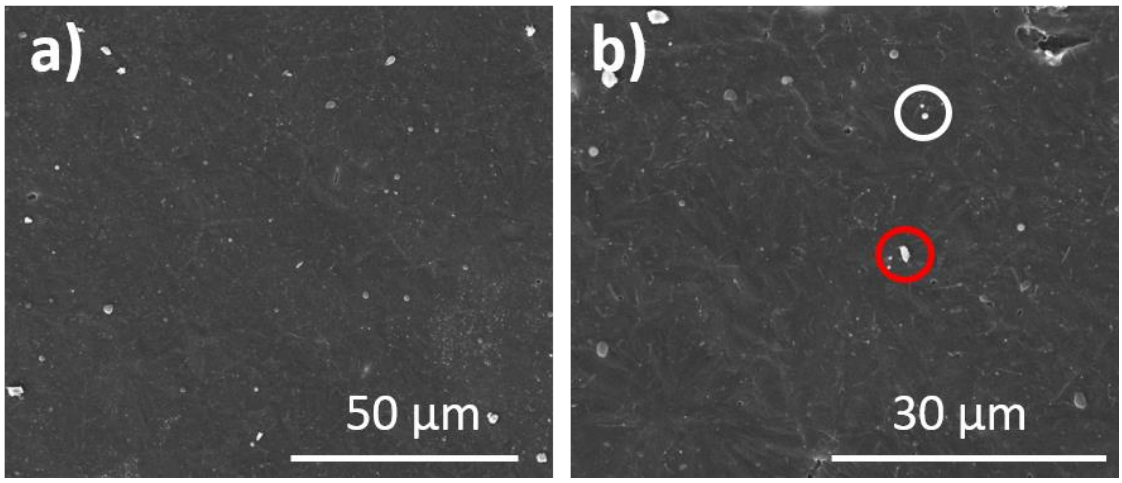

Figure 4.33. SEM images of *S. aureus* after 15 minutes of adhesion to 4 wt. % Ag NW/PLA nanocomposite disk.

Grown bacteria colonies after 15 minutes of incubation are shown in Figure 4.28. Dramatic decrease in bacterial concentration with Ag NW loading was obtained when incubated agar plates of bare PLA and 4 wt. % Ag NW/PLA were compared. However, bacterial reproduction could not be stopped completely, living bacteria colonies were still present on the agar even if they were only a few. This examination also supported the adhesion test results and the SEM images.

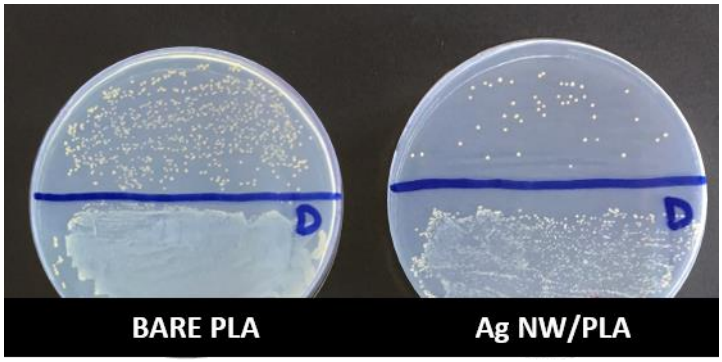

Figure 4.34. Photograph of incubated *S. aureus* colonies in agar plates after 15 minutes of adhesion with bare PLA (left) and 4 wt. % Ag NW/PLA (right).

4.3.3.2. Adhesion Test Against *Escherichia coli*

Adhesion test results against *E. coli* are plotted and provided in Figure 4.29. This graph primarily indicated that the bacteria can not completely hold onto the surface of bare PLA disks because of the reasons stated previously for *S. aureus*. Bacterial concentration on bare PLA fluctuated between 10^7 and 10^6 CFU/mL, which was used as the reference to reveal the antimicrobial performance of Ag NWs in PLA matrix.

Secondly, it was realised that, Ag ions inhibited *E. coli* to adhere and multiply on the disk surfaces. Bacterial concentration decreased rapidly down to almost 10^2 CFU/mL in 30 minutes with 4 wt. % Ag NW loading. After 30 minutes, the bacterial concentration was found to be increased with time but still remained much lower than the bacterial concentration of bare PLA. Moreover, lower Ag NW additions also showed antibacterial performance in 30 minutes of adhesion. However, maximum performance against *E. coli* was obtained for 4 wt. % Ag NW/PLA nanocomposite sample in 30 minutes. Based on these results it can be summarized that silver ion release of NWs and penetration to the cell wall was successfully achieved after 30 minutes and so, highest antimicrobial performance was obtained.

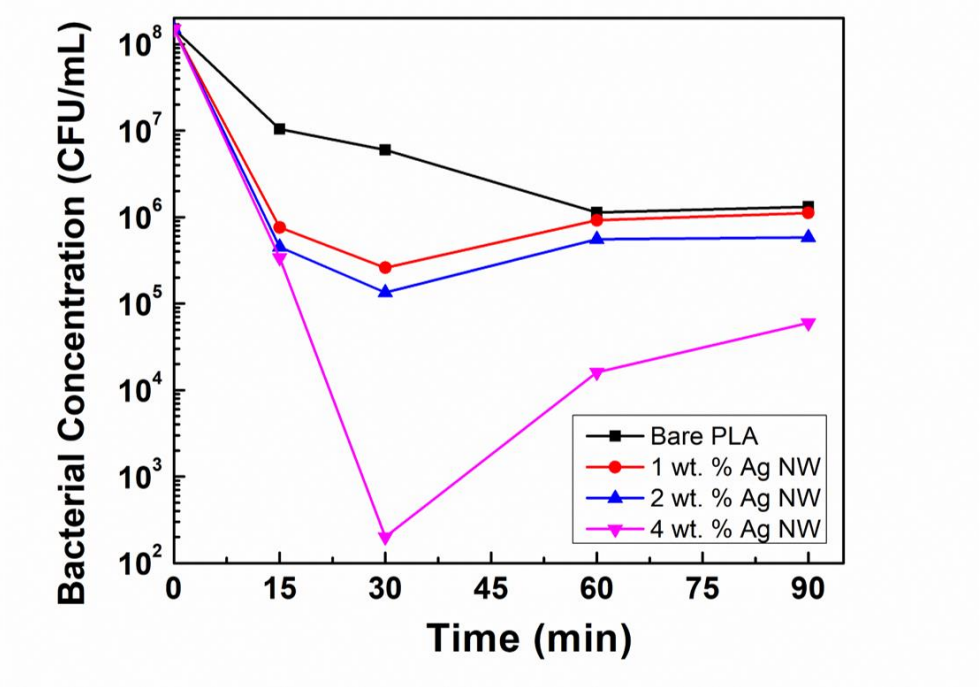

Figure 4.35. Change in bacterial concentration (CFU/mL) with time (min) after 15, 30, 60, 90 minutes of adhesion against *E. coli*.

Despite of Ag NWs in nanocomposites, it is shown in Figure 4.30 that bacterial colonies were started to hold on the surface with time, as demonstrated by white circles. At the same time, damaged and dead bacteria cells, circled by red, were also evident in the SEM image. This situation implies that NWs firstly prevented bacteria to hold on the surface and decreased bacterial concentration dramatically; however, after a while, bacterial concentrations held on the surface was increased slightly as expected based on the previous adhesion test results.

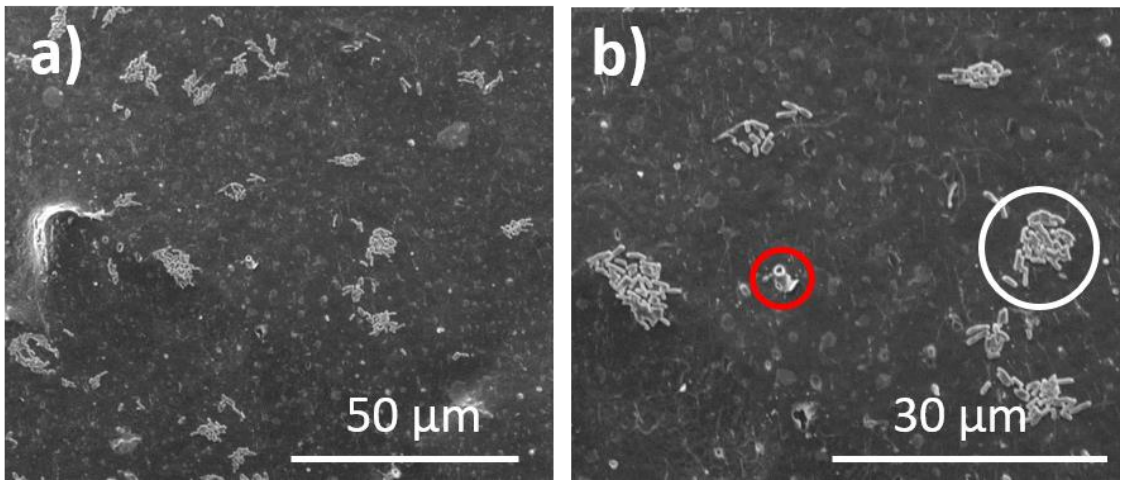

Figure 4.36. SEM images of growing *E. coli* bacteria after 90 minutes of adhesion to 4 wt. % Ag NW/PLA nanocomposite disk.

Bacterial colonies on agar plates are shown in Figure 4.31. It was realized that the bacterial concentration was much lower in Ag NW/PLA nanocomposites agar plate than that of bare PLA even after 90 minutes of adhesion. This revealed that the addition of Ag NWs improved the antibacterial behaviour of PLA against *E. coli* and maintained this effect at a reasonable level even though efficiency was diminished with adhesion time after 30 minutes.

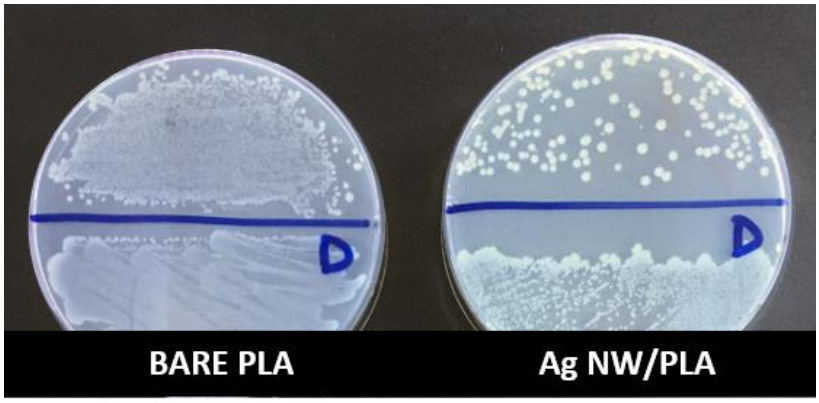

Figure 4.39. Photograph of incubated *Escherichia coli* colonies in agar plates after 90 minutes of adhesion with bare PLA (left) and 4 wt. % Ag NW/PLA (right).

CHAPTER 5

CONCLUSIONS AND FUTURE RECOMMENDATIONS

5.1. Conclusions

In this study, PLA based Ag NW nanocomposites were successfully prepared by the solution mixing method and 3D printed to get desired shapes. Morphological, thermal and antibacterial properties of 3D printed nanocomposites were investigated in detail. Ag NWs were homogenously distributed within the PLA matrix by solution mixing and highly aligned in the direction of shear force. After twin screw extrusion and 3D printing processes, it was noted that the NWs did get shorter and their alignment was lost.

TG analysis before and after 3D printing showed that the existence of NWs slightly delayed degradation of polymer matrix and also maintained its effect after 3D printing. Moreover, DSC results revealed that crystallinity increased remarkably with the addition of Ag NWs. At the same time, 3D printing process also improved the crystallinity of the polymer matrix.

Lastly and most importantly, antimicrobial performance of Ag NW loaded nanocomposites were evaluated. Disk diffusion method was carried out and reasonable results were obtained. Then, time kill assay and adhesion tests against *S. aureus* and *E. coli* were performed to evaluate killing capacity of Ag and adhesion capability of bacteria, respectively. It was realized that Ag NWs dramatically improve the antibacterial performances even at low loading levels. Time kill test results indicated 100% killing capacity against both *S. aureus* and *E. coli* in 2 hours. Moreover, 100% bactericidal effect was continued even after 24 hours against *E. coli* for all Ag NW loadings (1, 2, 4 wt. %). On the other hand, 100% killing capacity against *S. aureus* was observed up to 8 hours at the highest loading (4 wt. %).

Moreover, adhesion test results were found to be in good agreement with the time kill tests. As a result of antibacterial tests, it can be concluded that Ag NWs successfully prevented the bacterial reproduction and killed bacterial cells. In addition, results also showed that Ag NWs exhibited higher performance against *E. coli* as a Gram-negative basil rather than *S. aureus* because of the cell wall structure of the bacteria groups.

This study shows that Ag NW loaded PLA nanocomposites can perform bactericidal and bacteriostatic behavior against *E. coli* and *S.s aureus*, most common bacteria types living in public areas. Therefore, 3D printed Ag NW/PLA nanocomposites can be used in public areas and personal products that are used extensively on a daily basis. For example, places such as elevators, cash machines, toilet doors, faucet knobs, that are intensively used by masses and prone to significant bacterial reproduction can be covered by 3D printed antibacterial materials. Moreover, game consoles, mostly preferred by children in common use areas, hold large quantity of bacteria and can also be covered by a single use rigid case. Finally, personal products such as phone cases and key rings can be replaced easily with 3D printed Ag NW based nanocomposites developed in this work.

5.2. Further Recommendations

In this thesis, Ag NWs showed high antibacterial performance within the 3D printed nanocomposites even at low loading levels when compared to literature. Fabrication of this antibacterial material in the filament form would simply allow 3D printing of antibacterial products as desired and facilitate their integration into consumer products in large extent. In addition, in order to advance its performance and to keep the bactericidal effect for longer time intervals, Ag NW loadings can be increased for more sensitive conditions.

Secondly, Ag has been known for a long time as an antibacterial agent and this work was also focused on the antimicrobial performance of the Ag ions. On the other hand, NWs were found to enhance the mechanical performance of the polymer matrices in literature [71].

Therefore, Ag NWs can also be used to improve the mechanical strength of PLA, which in bare form exhibits highly brittle behavior. Moreover, the effect of print settings (printing pattern, infill content) on the behavior of 3D printed Ag NW/PLA nanocomposites can be investigated.

Thirdly, NWs are commonly used as nanofillers for the development of conductive polymer matrix composites. Therefore, Ag NW/PLA nanocomposites with higher NW loadings can be fabricated and used as conductive inks in 3D printers for different applications. For this case, it is important to prevent breaking of NWs during extrusion to create a percolative and thus conductive path. Therefore, twin screw extruders can be replaced by a single screw extruder to target electrical conductivity with high aspect ratio Ag NWs in nanocomposites.

REFERENCES

[1] X. Wang, M. Jiang, Z. Zhou, J. Gou, and D. Hui, "3D printing of polymer matrix composites: A review and prospective," *Compos. Part B Eng.*, vol. 110, pp. 442–458, 2017.

[2] W. S. W. Harun, M. S. I. N. Kamariah, N. Muhamad, S. A. C. Ghani, F. Ahmad, and Z. Mohamed, "A review of powder additive manufacturing processes for metallic biomaterials," *Powder Technol.*, vol. 327, pp. 128–151, 2018.

[3] M. Vitale, M. Cotteleer, and J. Holdowsky, "An Overview of Additive Manufacturing," *Def. AT&L November-December 2016 6*, no. December, pp. 6–13, 2016.

[4] B. M. Tymrak, M. Kreiger, and J. M. Pearce, "Mechanical properties of components fabricated with open-source 3-D printers under realistic environmental conditions," *Mater. Des.*, vol. 58, pp. 242–246, Jun. 2014.

[5] P. Tran, T. D. Ngo, A. Ghazlan, and D. Hui, "Bimaterial 3D printing and numerical analysis of bio-inspired composite structures under in-plane and transverse loadings," *Compos. Part B Eng.*, vol. 108, pp. 210–223, Jan. 2017.

[6] R. Melnikova, A. Ehrmann, and K. Finsterbusch, "3D printing of textile-based structures by Fused Deposition Modelling (FDM) with different polymer materials," *IOP Conf. Ser. Mater. Sci. Eng.*, vol. 62, p. 012018, Aug. 2014.

[7] Q. Sun, G. M. Rizvi, C. T. Bellehumeur, and P. Gu, "Effect of processing conditions on the bonding quality of FDM polymer filaments," *Rapid Prototyp. J.*, vol. 14, no. 2, pp. 72–80, Mar. 2008.

[8] L. Sha, Z. Chen, Z. Chen, A. Zhang, and Z. Yang, "Polylactic acid based nanocomposites: Promising safe and biodegradable materials in biomedical field," *Int. J. Polym. Sci.*, vol. 2016, 2016.

[9] R. P. Babu, K. O'Connor, and R. Seeram, "Current progress on bio-based polymers and their future trends," *Prog. Biomater.*, vol. 2, no. 1, p. 8, 2013.

[10] Z. Weng, J. Wang, T. Senthil, and L. Wu, "Mechanical and thermal properties of ABS/montmorillonite nanocomposites for fused deposition modeling 3D

printing," *Mater. Des.*, vol. 102, pp. 276–283, 2016.

[11] M. R. Skorski, J. M. Esenther, Z. Ahmed, A. E. Miller, and M. R. Hartings, "The chemical, mechanical, and physical properties of 3D printed materials composed of TiO2-ABS nanocomposites," *Sci. Technol. Adv. Mater.*, vol. 17, no. 1, pp. 89–97, 2016.

[12] J. R. Morones *et al.*, "The bactericidal effect of silver nanoparticles," *Nanotechnology*, vol. 16, no. 10, pp. 2346–2353, 2005.

[13] C. Elliott, "The effects of silver dressings on chronic and burns wound healing.," *Br. J. Nurs.*, vol. 19, no. 15, pp. S32-6, Aug. 2010.

[14] N. P. Aditya, P. G. Vathsala, V. Vieira, R. S. R. Murthy, and E. B. Souto, "Advances in nanomedicines for malaria treatment," *Adv. Colloid Interface Sci.*, vol. 201–202, pp. 1–17, Dec. 2013.

[15] S. Poulose, T. Panda, P. P. Nair, and T. Theodore, "Biosynthesis of silver nanoparticles.," *J. Nanosci. Nanotechnol.*, vol. 14, no. 2, pp. 2038–2049, Feb. 2014.

[16] A. Panacek *et al.*, "Silver colloid nanoparticles: synthesis, characterization, and their antibacterial activity.," *J. Phys. Chem. B*, vol. 110, no. 33, pp. 16248–16253, Aug. 2006.

[17] M. D. Kamyar Shameli, Mansor Bin Ahmad, Wan Md Zin Wan Yunus, Nor Azowa Ibrahim, Russly Abdul Rahman, Maryam Jokar, "Silver / poly (lactic acid) nanocomposites : preparation , characterization , and antibacterial activity," *Int. J. Nanomedicine*, pp. 573–579, 2010.

[18] L. Yu, Y. Zhang, B. Zhang, and J. Liu, "Enhanced antibacterial activity of silver nanoparticles/halloysite nanotubes/graphene nanocomposites with sandwich-like structure," *Sci. Rep.*, vol. 4, pp. 1–5, 2014.

[19] P. Enzymes, "United States Patent (19) 54," vol. 96, no. 19, pp. 62–66, 1980.

[20] T. D. Ngo, A. Kashani, G. Imbalzano, K. T. Q. Nguyen, and D. Hui, "Additive manufacturing (3D printing): A review of materials, methods, applications and challenges," *Compos. Part B Eng.*, vol. 143, no. February, pp. 172–196, 2018.

[21] S. C. Ligon, R. Liska, J. Stampfl, M. Gurr, and R. Mülhaupt, "Polymers for 3D Printing and Customized Additive Manufacturing," *Chem. Rev.*, vol. 117, no. 15, pp. 10212–10290, 2017.

[22] N. S. A. Bakar, M. R. Alkahari, and H. Boejang, "Analysis on fused deposition modelling performance," *J. Zhejiang Univ. A*, vol. 11, no. 12, pp. 972–977,

Dec. 2010.

[23] B. Brenken, E. Barocio, A. Favaloro, V. Kunc, and R. B. Pipes, “Fused filament fabrication of fiber-reinforced polymers: A review,” *Addit. Manuf.*, vol. 21, no. February, pp. 1–16, 2018.

[24] O. A. Mohamed, S. H. Masood, and J. L. Bhowmik, “Optimization of fused deposition modeling process parameters for dimensional accuracy using I-optimality criterion,” *Measurement*, vol. 81, pp. 174–196, Mar. 2016.

[25] A. K. Sood, R. K. Ohdar, and S. S. Mahapatra, “Parametric appraisal of mechanical property of fused deposition modelling processed parts,” *Mater. Des.*, vol. 31, no. 1, pp. 287–295, Jan. 2010.

[26] J. S. Chohan, R. Singh, K. S. Boparai, R. Penna, and F. Fraternali, “Dimensional accuracy analysis of coupled fused deposition modeling and vapour smoothing operations for biomedical applications,” *Compos. Part B Eng.*, vol. 117, pp. 138–149, May 2017.

[27] V. Bhavar, P. Kattire, V. Patil, S. Khot, K. Gujar, and R. Singh, “A Review on Powder Bed Fusion Technology of Metal Additive Manufacturing,” *4th Int. Conf. Exhib. Addit. Manuf. Technol.*, pp. 1–2, 2014.

[28] H. Lee, C. H. J. Lim, M. J. Low, N. Tham, V. M. Murukeshan, and Y. J. Kim, “Lasers in additive manufacturing: A review,” *Int. J. Precis. Eng. Manuf. - Green Technol.*, vol. 4, no. 3, pp. 307–322, 2017.

[29] B. Utela, D. Storti, R. Anderson, and M. Ganter, “A review of process development steps for new material systems in three dimensional printing (3DP),” *J. Manuf. Process.*, vol. 10, no. 2, pp. 96–104, Jul. 2008.

[30] F. P. W. Melchels, J. Feijen, and D. W. Grijpma, “A review on stereolithography and its applications in biomedical engineering,” *Biomaterials*, vol. 31, no. 24, pp. 6121–6130, Aug. 2010.

[31] S. Singh, S. Ramakrishna, and R. Singh, “Material issues in additive manufacturing: A review,” *J. Manuf. Process.*, vol. 25, pp. 185–200, 2017.

[32] J. R. C. Dizon, A. H. Espera, Q. Chen, and R. C. Advincula, “Mechanical characterization of 3D-printed polymers,” *Addit. Manuf.*, vol. 20, pp. 44–67, 2018.

[33] Y. H. Cho, I. H. Lee, and D.-W. Cho, “Laser scanning path generation considering photopolymer solidification in micro-stereolithography,” *Microsyst. Technol.*, vol. 11, no. 2, pp. 158–167, Feb. 2005.

[34] C. Heller, M. Schwentenwein, G. Russmueller, F. Varga, J. Stampfl, and R. Liska, “Vinyl esters: Low cytotoxicity monomers for the fabrication of biocompatible 3D scaffolds by lithography based additive manufacturing,” *J. Polym. Sci. Part A Polym. Chem.*, vol. 47, no. 24, pp. 6941–6954.

[35] K. S. Prakash, T. Nancharaih, and V. V. S. Rao, “Additive Manufacturing Techniques in Manufacturing -An Overview,” *Mater. Today Proc.*, vol. 5, no. 2, pp. 3873–3882, 2018.

[36] J. Manapat, Q. Chen, P. Ye, and R. Advincula, “3D Printing of Polymer Nanocomposites via Stereolithography,” *Macromol. Mater. Eng.*, vol. 302, p. 1600553, 2017.

[37] A. C. De Leon, Q. Chen, N. B. Palaganas, J. O. Palaganas, J. Manapat, and R. C. Advincula, “High performance polymer nanocomposites for additive manufacturing applications,” *React. Funct. Polym.*, vol. 103, pp. 141–155, 2016.

[38] W. H. Carothers and J. W. Hill, “Studies of Polymerization and Ring Formation. XV. Artificial Fibers from Sythetic Linear Condensation Superpolymers,” *J. Am. Chem. Soc.*, vol. 54, no. 4, pp. 1579–1587, Apr. 1932.

[39] D. Garlotta, “A Literature Review of Poly(Lactic Acid),” *J. Polym. Environ.*, vol. 9, no. 2, pp. 63–84, Apr. 2001.

[40] J. M. Raquez, Y. Habibi, M. Murariu, and P. Dubois, “Polylactide (PLA)-based nanocomposites,” *Prog. Polym. Sci.*, vol. 38, no. 10–11, pp. 1504–1542, 2013.

[41] E. T. H. Vink and S. Davies, “Life Cycle Inventory and Impact Assessment Data for 2014 Ingeo ™ Polylactide Production,” *Ind. Biotechnol.*, vol. 11, no. 3, pp. 167–180, 2015.

[42] R. Drumright, P. R. Gruber, and D. E. Henton, “Polylactic Acid Technology,” *Adv. Mater.*, vol. 12, pp. 1841–1846, 2000.

[43] E. T. H. Vink, K. R. Rábago, D. A. Glassner, and P. R. Gruber, “Applications of life cycle assessment to NatureWorks™ polylactide (PLA) production,” *Polym. Degrad. Stab.*, vol. 80, no. 3, pp. 403–419, Jan. 2003.

[44] K. Masutani and Y. Kimura, “Chapter 1 PLA Synthesis. From the Monomer to the Polymer,” pp. 1–36, 2015.

[45] D. W. Farrington, J. Lunt, and S. Davies, “Poly(lactic acid) fibers,” *Biodegrad. Sustain. Fibres*, pp. 191–220, Jan. 2005.

[46] S. Sosnowski, M. Gadzinowski, and S. Slomkowski, “Poly(l,l-lactide)

Microspheres by Ring-Opening Polymerization," *Macromolecules*, vol. 29, no. 13, pp. 4556–4564, 1996.

[47] I. Engelberg and J. Kohn, "Physico-mechanical properties of degradable polymers used in medical applications: a comparative study.," *Biomaterials*, vol. 12, no. 3, pp. 292–304, Apr. 1991.

[48] H. Tsuji and Y. Ikada, "Stereocomplex formation between enantiomeric poly(lactic acid)s. XI. Mechanical properties and morphology of solution-cast films," *Polymer (Guildf).*, vol. 40, no. 24, pp. 6699–6708, Nov. 1999.

[49] G. Perego, G. Domenico Cella, and C. Bastioli, "Effect of molecular weight and crystallinity on poly(lactic acid) mechanical properties," *J. Appl. Polym. Sci.*, vol. 59, pp. 37–43, 1996.

[50] D. W. Grijpma and A. J. Pennings, "(Co)polymers of L-lactide, 2. Mechanical properties," *Macromol. Chem. Phys.*, vol. 195, pp. 1649–1663, 1994.

[51] P. Törmälä, "Biodegradable self-reinforced composite materials; Manufacturing structure and mechanical properties," *Clin. Mater.*, vol. 10, no. 1–2, pp. 29–34, Jan. 1992.

[52] S. Jacobsen and H. G. Fritz, "Plasticizing polylactide?the effect of different plasticizers on the mechanical properties," *Polym. Eng. Sci.*, vol. 39, no. 7, pp. 1303–1310, 1999.

[53] K. Van de Velde and P. Kiekens, "Biopolymers: overview of several properties and consequences on their applications," *Polym. Test.*, vol. 21, no. 4, pp. 433–442, Jan. 2002.

[54] I. Ovid'ko, "Mechanical Properties of Graphene," *Rev. Adv. Mater. Sci.*, vol. 34, pp. 1–11, 2013.

[55] K. Prashantha and F. Roger, "Multifunctional properties of 3D printed poly(lactic acid)/graphene nanocomposites by fused deposition modeling," *J. Macromol. Sci. Part A Pure Appl. Chem.*, vol. 54, no. 1, pp. 24–29, 2017.

[56] J. Bustillos, D. Montero, P. Nautiyal, A. Loganathan, B. Boesl, and A. Agarwal, "Integration of graphene in poly(lactic) acid by 3D printing to develop creep and wear-resistant hierarchical nanocomposites," *Polym. Compos.*, vol. 0, no. 0.

[57] K. Chizari, M. A. Daoud, A. R. Ravindran, and D. Therriault, "3D Printing of Highly Conductive Nanocomposites for the Functional Optimization of Liquid Sensors," *Small*, vol. 12, no. 44, pp. 6076–6082, 2016.

[58] B. Coppola, N. Cappetti, L. Di Maio, P. Scarfato, and L. Incarnato, “Layered silicate reinforced polylactic acid filaments for 3D printing of polymer nanocomposites,” *RTSI 2017 - IEEE 3rd Int. Forum Res. Technol. Soc. Ind. Conf. Proc.*, pp. 3–6, 2017.

[59] N. Beyth, Y. Houri-Haddad, A. Domb, W. Khan, and R. Hazan, “Alternative antimicrobial approach: Nano-antimicrobial materials,” *Evidence-based Complement. Altern. Med.*, vol. 2015, 2015.

[60] M. Rai, A. Yadav, and A. Gade, “Silver nanoparticles as a new generation of antimicrobials,” *Biotechnol. Adv.*, vol. 27, no. 1, pp. 76–83, Jan. 2009.

[61] W. R. Li, X. B. Xie, Q. S. Shi, H. Y. Zeng, Y. S. Ou-Yang, and Y. Ben Chen, “Antibacterial activity and mechanism of silver nanoparticles on Escherichia coli,” *Appl. Microbiol. Biotechnol.*, vol. 85, no. 4, pp. 1115–1122, 2010.

[62] I. Sondi and B. Salopek-Sondi, “Silver nanoparticles as antimicrobial agent: a case study on E. coli as a model for Gram-negative bacteria,” *J. Colloid Interface Sci.*, vol. 275, no. 1, pp. 177–182, Jul. 2004.

[63] K.-H. Cho, J.-E. Park, T. Osaka, and S.-G. Park, “The study of antimicrobial activity and preservative effects of nanosilver ingredient,” *Electrochim. Acta*, vol. 51, no. 5, pp. 956–960, Nov. 2005.

[64] K. Zheng, M. I. Setyawati, D. T. Leong, and J. Xie, “Antimicrobial silver nanomaterials,” *Coord. Chem. Rev.*, vol. 357, pp. 1–17, 2018.

[65] R. Kalaivani *et al.*, “Synthesis of chitosan mediated silver nanoparticles (Ag NPs) for potential antimicrobial applications,” *Front. Lab. Med.*, vol. 2, no. 1, pp. 30–35, 2018.

[66] S. Coskun, B. Aksoy, and H. Unalan, “Polyol Synthesis of Silver Nanowires: An Extensive Parametric Study,” *Cryst. Growth Des.*, vol. 11, pp. 4963–4969, 2011.

[67] M. Kaláb, A. Yang, and D. Chabot, “Conventional Scanning Electron Microscopy of Bacteria,” *Infocus*, pp. 44–61, 2008.

[68] Particle Sciences, “Hot Melt Extrusion,” *Tech. Br. 2011 vol. 3*, vol. 3, p. 2, 2011.

[69] A. Eda, “Poly (Lactic acid) based nanocomposites: mechanical, thermal and reological properties and morphology,” *Middle East Tech. Univ.*, no. July, p. 261, 2014.

[70] A. Grémare *et al.*, “Characterization of printed PLA scaffolds for bone tissue

engineering," *J. Biomed. Mater. Res. - Part A*, vol. 106, no. 4, pp. 887–894, 2018.

[71] D. Doganay, S. Coskun, C. Kaynak, and H. Unalan, "Electrical, mechanical and thermal properties of aligned silver nanowire/polylactide nanocomposite films," *Compos. Part B Eng.*, vol. 99, 2016.

[72] C. Yang, X. Tian, D. Li, Y. Cao, F. Zhao, and C. Shi, "Influence of thermal processing conditions in 3D printing on the crystallinity and mechanical properties of PEEK material," *J. Mater. Process. Technol.*, vol. 248, no. May, pp. 1–7, 2017.

[73] K. Gnanasekaran *et al.*, "3D printing of CNT- and graphene-based conductive polymer nanocomposites by fused deposition modeling," *Appl. Mater. Today*, vol. 9, pp. 21–28, 2017.

[74] I. R. Mustapa, R. A. Shanks, and I. Kong, "Melting Behaviour and Dynamic Mechanical Properties of Poly (lactic acid) -Hemp-Nanosilica Composites," vol. 03, no. 02, pp. 29–37, 2013.

[75] D. Battegazzore, S. Bocchini, and A. Frache, "Crystallization kinetics of poly(lactic acid)-talc composites," *Express Polym. Lett.*, vol. 5, no. 10, pp. 849–858, 2011.

[76] M. A. Cuiffo, J. Snyder, A. M. Elliott, N. Romero, S. Kannan, and G. P. Halada, "Impact of the Fused Deposition (FDM) Printing Process on Polylactic Acid (PLA) Chemistry and Structure," *Appl. Sci.*, vol. 7, no. 6, p. 579, 2017.

[77] R. Coico, "Gram staining.," *Curr. Protoc. Microbiol.*, vol. Appendix 3, p. Appendix 3C, Oct. 2005.

[78] I. S. Tan and K. S. Ramamurthi, "Spore formation in Bacillus subtilis," vol. 6, no. 3, pp. 212–225, 2014.

[79] D. Mosselhy *et al.*, "Nanosilver–Silica Composite: Prolonged Antibacterial Effects and Bacterial Interaction Mechanisms for Wound Dressings," *Nanomaterials*, vol. 7, no. 9, p. 261, 2017.

[80] D. P. Tamboli and D. S. Lee, "Mechanistic antimicrobial approach of extracellularly synthesized silver nanoparticles against gram positive and gram negative bacteria," *Journal of Hazardous Materials*, vol. 260. pp. 878–884, 2013.

[81] H. Lee, D. Ryu, S. Choi, and D. Lee, "Antibacterial Activity of Silver-nanoparticles Against Staphylococcus aureus and Escherichia coli," *Korean J.*

Microbiol. Biotechnol., vol. 39, no. 1, pp. 77–85, 2011.

[82] W. K. Jung, H. C. Koo, K. W. Kim, S. Shin, S. H. Kim, and Y. H. Park, "Antibacterial Activity and Mechanism of Action of the Silver Ion in Staphylococcus aureus and Escherichia coli," *Appl. Environ. Microbiol.*, vol. 74, no. 7, pp. 2171–2178, 2008.

[83] T. C. Dakal, A. Kumar, R. S. Majumdar, and V. Yadav, "Mechanistic basis of antimicrobial actions of silver nanoparticles," *Front. Microbiol.*, vol. 7, no. NOV, pp. 1–17, 2016.

[84] L.-T. Lim, R. Auras, and M. Rubino, "Processing technologies for poly(lactic acid)," *Prog. Polym. Sci.*, vol. 33, no. 8, pp. 820–852, Aug. 2008.